

NASA Technical Paper 1614

NASA
TP
1610-
v.2
c.1

LOAN COPY
AFWL TECH
KIRTLAND A

0134844



Aerodynamic Performances of Three Fan Stator Designs Operating With Rotor Having Tip Speed of 337 Meters Per Second and Pressure Ratio of 1.54

II - Relation of Analytical Code Calculations to Experimental Performance

Thomas F. Gelder, James F. Schmidt,
and Genevieve M. Esgar

APRIL 1980

NASA



NASA Technical Paper 1614

Aerodynamic Performances of Three Fan Stator Designs Operating With Rotor Having Tip Speed of 337 Meters Per Second and Pressure Ratio of 1.54

II - Relation of Analytical Code Calculations to Experimental Performance

Thomas F. Gelder, James F. Schmidt,
and Genevieve M. Esgar
*Lewis Research Center
Cleveland, Ohio*



National Aeronautics
and Space Administration

**Scientific and Technical
Information Office**

1980

CONTENTS

	Page
SUMMARY	1
INTRODUCTION	1
ANALYTICAL TECHNIQUES	3
Hub-to-Shroud Code (MERIDL)	3
Blade-to-Blade Code (TSONIC)	4
Application and Limitations of Codes	5
RESULTS AND DISCUSSION	7
Inviscid Flow Calculations - Hub-to-Shroud Solutions	7
Midchannel velocities	7
Streamtube heights	9
Analytical results versus data	9
Inviscid Flow Calculations - Blade-to-Blade Solutions	10
Surface velocities from TSONIC	10
Surface velocities - comparison of calculation methods	13
Loss Correlations	14
Background	14
Using velocities from internal-flow analysis calculations	15
Using velocities from diagrams at blade inlet and outlet and comparisons with internal-flow analysis.	16
Estimating blade maximum suction-surface velocity at off-design operation . .	17
Using Analysis Codes in Design	19
CONCLUDING REMARKS	21
SUMMARY OF RESULTS	21
APPENDIX - SYMBOLS	23
REFERENCES	25

SUMMARY

A hub-to-shroud, and a blade-to-blade internal-flow-analysis code, both inviscid and basically subsonic, were used to calculate flow parameters within four different stator-blade rows. Some relations between these internal flow calculations and conventionally obtained performance results were established. Three different stator designs were involved in the study, but each was operated with the same rotor.

One stator design was that of the NASA QF-1 fan stage. For the present studies test results from a 0.5-meter-diameter scale model of it were used. This stator had 112 blades, a short chord of 1.85 centimeter, and an aspect ratio of 5.1. It was tested at two different setting angles. The rotor had a design tip speed of 337 meters per second and a pressure ratio of 1.54.

The second and third stator designs each had 60 blades, moderate chords of 3.72 centimeters, and aspect ratios of 2.6. The second design was based on a minimum-lift-fluctuation theory of noise reduction. The third was patterned after an aerodynamically successful stator developed under NASA contract.

The internal-flow-analysis-code calculated ratio of maximum-suction-surface velocity to trailing-edge velocity (suction-surface diffusion ratio) correlated well, in the midspan region (30 to 70 percent span), with the measured total-loss parameters over the minimum-loss to near-stall operating range for all stators and speeds studied.

It is also shown that adding a simple incidence-angle term to velocity-diagram estimates of the suction-surface diffusion ratios improves their accuracy, which in turn provides a minimum-loss to near-stall-loss correlation comparable with that obtained with the internal-flow analysis calculations.

To illustrate the potential benefits of a blade designed with the aid of the present flow-analysis codes, a redesign of the original QF-1 short-chord stator is proposed. For the same chord length and number of blades, geometry and incidence angle were changed to minimize the maximum suction-surface velocity at each blade section. An overall efficiency improvement of 1.6 points above the peak previously measured with the original design is predicted for the redesign.

INTRODUCTION

Analysis of the aerodynamic performance of fan or compressor blading is usually dependent on interpreting data that are measured upstream and downstream of the blade

row. This is typically done along streamlines at several spanwise locations to assess the flow differences from hub-to-shroud. However, it has long been recognized that detailed knowledge of flow conditions within and on the blade row would significantly improve analysis capability and provide added design control.

In recent years flow-analysis codes have been written for high-speed digital computers that can rapidly calculate blade surface velocities and other flow details within the blade row. To do this, flow conditions upstream and downstream of the blade row are used as input boundary values. The codes presently available generally simplify in various ways the complex, real flow through fan or compressor blading. By using some of the codes sequentially, improved approximations to the actual flow can be made.

Analysis-code calculations have the potential of predicting many performance features of interest such as blade-element loss and deviation angle, blade-row pressure ratio and efficiency, and near-stall or near-choke operating conditions. These codes may also indicate directions for performance improvement. Of course the accuracy of such performance predictions depends on the degree of reality that is embodied (or required) in the assumptions and flow modeling used in the codes. There are strong incentives to improve the reliability of compressor-design systems; chief among them is the desire to reduce or eliminate costly trial and error experiments with complex hardware. Increased use of internal-flow analysis during the design process has the greatest potential for achieving this improvement. Also, the analysis codes may identify more reliable parameters with which to correlate experimental data.

In the present report a hub-to-shroud and a blade-to-blade flow analysis code were used to calculate the flow parameters within four different, previously tested stator-blade rows representing three different stator designs. These codes are two-dimensional, inviscid, and basically for subsonic flows. The codes' input boundary values are provided by experimental data or by design predictions which are detailed in Part I of this report (ref. 1). Briefly, the stators were all designed to operate behind the same rotor and in essentially the same overall flow path. The rotor and flow path were a 0.5-meter-diameter scale model of the NASA QF-1 fan (ref. 2). All stator-blade sections were of the multiple-circular-arc family (ref. 3). One stator design, the original for NASA QF-1, has been studied at two setting angles (ref. 2): at the design setting angle it is called S9 and at the other angle it is called S9R, for S9 reset. The second design, S9C, was based on a minimum lift-fluctuation theory of noise reduction (refs. 4 and 5). The third design, S9D, was patterned after an aerodynamically successful stator developed under NASA contract (ref. 6). The experimental performances of all these stators (based on the flow survey data taken outside the blade rows) are compared and discussed in reference 1.

For the present report, a hub-to-shroud analysis code (ref. 7) was first used to calculate the flow parameters on a midchannel stream surface. Then a blade-to-blade analysis code (ref. 8) calculated the flows on selected stream surfaces from hub-to-

shroud. Midchannel and blade-surface velocities calculated by these codes are presented for a broad range of operating conditions and spanwise locations.

The main purposes of the present report (Part II) are (1) to relate inviscid, two-dimensional, code-calculated, blade-surface velocities to measured losses in total pressure and to compare these with traditional methods of loss prediction and (2) to illustrate the potential benefits of a blade designed with the aid of internal-flow analysis codes by proposing a redesign of the original NASA QF-1 stator and predicting its improved performance.

The symbols used are defined in the appendix. All work was done at the NASA Lewis Research Center.

ANALYTICAL TECHNIQUES

Details of the hub-to-shroud and the blade-to-blade analysis codes are given in references 7 and 8, respectively. Only a brief description of each code will be given here, followed by a section on their application and limitations with the present data.

Hub-to-Shroud Code (MERIDL)

The basic analysis consists of the solution of the finite-difference equations of the stream function. The solution is on a hub-to-shroud midchannel stream surface of a turbomachinery blade row. It has the same shape as the blade mean camber surface except near the leading and trailing edges. There, arbitrary transition surfaces are required to match the free-stream flow. The computer code written to perform these internal-flow calculations is called MERIDL. The MERIDL solution represents a blade-to-blade average of flow properties. The basic solution is limited to subsonic flow, compressible and shock free. This was sufficient for the present study. (If there is locally supersonic flow, a transonic solution is estimated by combining the stream-function solution with a velocity-gradient solution; see ref. 7.)

The required geometric inputs are the hub and shroud coordinates and the blade-section geometry from hub to shroud. These inputs are generated from the Lewis blade-design program (ref. 3). The finite-difference solution mesh is also specified.

The required aerodynamic inputs are the weight flow, the radial distribution of blade relative values of inlet total temperature, inlet and outlet total pressure, and inlet and outlet tangential velocity. Their source is the experimental data or from design or off design programs that predict performance. For the present analysis both were used. When experimental data were used, the flow measurements taken between 5- and 95-percent span (ref. 1) were faired to the hub and shroud. In particular, the dropoff

in total pressure observed in the end-wall regions due to wall boundary layers was continued, rather arbitrarily, to the walls. In this way the end-wall blockage effects were acknowledged. Also, an approximate correction for loss of total pressure through the blade row is provided in the MERIDL code. Here, measured loss in total pressure was assumed to be linearly distributed from leading to trailing edge.

The principal outputs of MERIDL are (1) the location of streamlines through the blade row at specified flow fractions from the hub, (2) the velocities and stream-tube-height distribution along each streamline, and (3) the radial distribution of blade-to-blade average velocities, flow angles, pressures, and temperatures at specified axial locations throughout the flow field. The MERIDL analysis also provides an estimate of the chordwise distribution of surface velocities for each specified streamline. It assumes a linear distribution of internal velocities between the suction and pressure surfaces. A comparison of these surface velocities from MERIDL with those subsequently calculated by a blade-to-blade code is presented in the RESULTS AND DISCUSSION section.

Blade-to-Blade Code (TSONIC)

The method developed in reference 8 to obtain a transonic flow solution on a blade-to-blade stream surface between blades of a turbomachine involves two phases of calculation. The first phase is to obtain a finite-difference solution of the stream function. Such a solution is limited to completely subsonic flow. The actual weight flow is reduced, if necessary, to satisfy this requirement. The second phase is to obtain a velocity distribution based on the actual weight flow by means of a velocity-gradient equation. The finite-difference solution at a reduced weight flow provides information needed to obtain the velocity-gradient solution. The resulting transonic solution, with the code name of TSONIC, is for compressible, shock-free flow.

The required geometric inputs to TSONIC are the blade-section geometry and the stream-tube height distribution for each blade-to-blade stream surface. The finite-difference solution mesh is also specified. The stream surfaces of interest are those previously selected for - and calculated by - MERIDL. Part of the MERIDL code output is precisely the blade-section geometry and stream-tube-height distribution required for TSONIC input.

The required aerodynamic inputs are the weight flow, the inlet total temperature and density, and the inlet and outlet flow angles relative to the blade. As with MERIDL, experimental data or design predictions provided these inputs for the present study.

The output of TSONIC provides blade-surface velocities, velocities and flow angles at all internal mesh points, and streamline coordinates and directions on the selected blade-to-blade stream surfaces.

Application and Limitations of Codes

As previously stated, a main purpose of this report is to relate inviscid, two-dimensional, code-calculated blade-surface velocities to measured losses in total pressure. Initial analysis of the present stator loss data indicated a good correlation with simply the magnitude of the maximum velocity diffusion on the suction surface. This diffusion was defined as the code-calculated ratio of maximum suction-surface velocity to trailing-edge velocity. For reasons later discussed, the trailing-edge velocity is not a blade-surface value calculated from TSONIC, but a blade-to-blade average from MERIDL.

Although only the maximum suction-surface and trailing-edge velocities calculated by the codes are used for the present loss correlations, other surface values were determined. They are of general interest and could be used for additional analyses. These could involve boundary-layer calculations and performance parameters other than loss. Therefore, the surface-velocity distributions over both suction and pressure surfaces are presented.

For each stator design and operating point of interest, one MERIDL calculation was made. Ten flow fractions from hub to shroud were specified to provide stream lines at 11 particular spanwise locations. Five of these locations, at the stator inlet of 10-, 30-, 50-, 70-, and 90-percent span, were selected for further study. A TSONIC calculation was then made at each of these spanwise locations for each operating point. No blockage factors were added to the walls or blade contours to represent any boundary-layer displacement thicknesses.

Because of the good loss correlation with the relatively simple approach previously described, it was considered unnecessary for present purposes to complicate the analysis process with boundary-layer calculations or iterations between the inviscid codes. This was highly desirable considering the number of stator designs, operating points, and spanwise locations involved. Of course, such refinements, when perfected, should improve the understanding of the loss mechanisms and result in more accurate and reliable loss predictions.

The TSONIC code calculations of blade-surface velocities have previously been compared with experimental values deduced from blade-surface static-pressure measurements (ref. 9). There, the midspan location of a compressor stator (inlet Mach number of 0.57) was analyzed. It showed that, using the actual stator-blade shape (a double-circular section in this case) and the measured exit flow angle, velocity distributions on the suction and pressure surfaces were in good agreement with measurements over the forward, nonseparated-flow portion of the chord. This was to at least 80 percent chord on the suction surface and over the entire pressure surface. However, around 92 percent chord, the TSONIC calculated velocity curves for suction and pressure surfaces

crossed. Similar results were obtained when the present data were used as input to TSONIC.

Obviously, the real flow over the last 10- to 20-percent chord is improperly modeled by the inviscid codes. Further analysis (ref. 9) with the stator-blade shape enlarged by a calculated boundary-layer displacement thickness eliminated the previously calculated crossing of surface velocities forward of 100 percent chord. However, unrealistic values of surface velocity were still calculated in the trailing-edge region. Other, empirical techniques for approximating surface velocities near the trailing edge are discussed in reference 9, but none of these were used here.

As previously indicated, the blade-trailing-edge velocities used in subsequent loss correlations were from MERIDL. It calculates an axisymmetric average (blade-to-blade) of the flow velocity at the trailing edge.

The maximum suction-surface Mach number of the reference 9 stator was about 0.9. For the present study comparable values as high as 1.3 are indicated in the hub region. The present code-calculated surface Mach numbers become less accurate as values increase above 1.0 because of the solution technique used (as previously described). The supersonic Mach number limits of the TSONIC code have not been clearly established. However, some comparisons with data (unpublished) indicate that peak suction-surface Mach numbers near 1.2 would be reasonably well predicted so long as a choked flow passage is not indicated. Surface velocities calculated downstream of such a supersonic peak would be more suspect however, because of the shock free and inviscid flow assumptions in the code.

Another approximation in using the MERIDL code is its specification of the mid-channel flow surface (ref. 7). It is somewhat arbitrary, as previously indicated. A limited study was made in which another midchannel surface was specified. It distributed the total air turning at the same rate chordwise as the change in blade mean camber line. The resulting surface velocities were hardly changed from the subsequent TSONIC calculation.

The quality of the TSONIC-calculated surface velocities in this report are summarized as follows: The maximum suction-surface velocities are believed reasonably close approximations to the real flow values. In addition, the surface-velocity distributions forward of any flow separation location (not estimated herein) and for subsonic surface Mach numbers are also considered reliable. Maximum suction-surface Mach numbers as high as 1.2 are also believed realistic, provided the flow passage has not choked. From the trailing edge forward to any flow-separation location, the calculated surface velocities cannot be correct because of the inviscid assumptions used. Finally, surface velocities in the midspan region (30- to 70-percent span) are considered more reliable than those in the end-wall regions (10- and 90-percent span) because of the two-dimensional nature of the flow and codes.

RESULTS AND DISCUSSION

Inviscid Flow Calculations - Hub-to-Shroud Solutions

Midchannel velocities. - From design value inputs the resulting midchannel velocities are plotted as a function of meridional distance from the leading edge (fig. 1). Five spanwise locations (10-, 30-, 50-, 70-, and 90-percent) are shown for each of the three stator designs (S9, S9C, and S9D). Although the MERIDL solution is done for a mid-channel surface that is generally at some varying angle to any radial-axial plane, the resulting output is presented as a function of distance on this plane. A percent-chord scale can also be projected into this meridional plane and such is included on this and other figures. Besides velocities, blade-section-centerline turning rates are shown for the inlet and outlet segments of the blade. They change at the transition location noted. Values of inlet and outlet camber in degrees are also given, as are the blade-section incidence angles, i_{mc} . The arrowheads shown on the velocity scales at the leading and trailing edges are the design values calculated by MERIDL.

In general, the leading-edge velocities increase from about 250 meters per second near the tip to about 290 meters per second near the hub. The trailing-edge velocities are about 200 meters per second across the span. Thus, the overall midchannel velocity gradient is steeper near the hub than the tip for all three stators. And, of course, the gradients are steeper for the shorter chord S9 (fig. 1(a)) than for the longer chord S9C or S9D.

At each spanwise location the total air turning is the same for all stator designs. Therefore, because deviation angles were nearly the same for all designs (see ref. 1, fig. 4(c)), incidence angle plus total camber at each location are about the same. Now, S9D does most of the air turning with blade camber (fig. 1(c)), whereas S9 uses less camber but much more incidence angle (fig. 1(a)). As expected, the peak midchannel velocity tends to be higher with the higher-incidence-angle S9 design.

The manner in which the midchannel velocity is diffused from leading to trailing edge along a streamline depends on the incidence angle of the oncoming flow and on the details of the blade geometry. Of the numerous blade-geometry choices available to the designer of a multiple-circular-arc (MCA) blade section (ref. 3), the inlet- and outlet-segment turning rates, and their transition location, are two that have significant influence on the local velocity gradient. For example, inflections in the velocity distribution are related to the change in turning rates at the transition locations for most of the blade sections shown. These inflections are particularly strong when the change in turning is large and when it goes from a higher value for the inlet segment to a lower one for the outlet segment. This is best illustrated by the S9C design (fig. 1(b)). In contrast, the velocity inflections are less for S9D (fig. 1(c)), where turning rates change from lower to higher values across the span.

In addition to the velocity gradients and inflections just discussed, the MCA blade sections have long been tailored to control velocity levels. Such MCA sections were initially developed for transonic flows so that accelerations to supersonic levels could be limited to avoid high shock losses. This was done by limiting the amount of inlet segment camber (product of inlet turning rate and surface distance to transition). This approach was used in the S9D design and resulted in the relatively low inlet camber shown near the hub. Other design considerations, like choke margins and throat locations, are also affected by MCA turning rates and transition locations. And these considerations may favor somewhat higher inlet segment cambers.

As might be expected and as will be shown in subsequent figures, the blade surface velocities tend to have similar chordwise patterns and gradients as the midchanned values. Thus, these MERIDL calculations (fig. 1) provide the first opportunity in the design process to exercise some control over the surface-velocity peaks and diffusion gradients across the complete blade span. Much of this control is through the selection of incidence angles, turning rates, and transition locations. Blade thickness distributions, chordwise and spanwise, also have some influence. For the inlet Mach number levels and MCA blades of this study, the thinnest possible blades appear best, and, generally, structural and/or fabrication requirements set these limits.

To minimize losses, the designer would usually prefer as low a peak midchannel velocity as possible and a smooth velocity diffusion to the trailing edge. Generally, re-accelerations should be avoided as well as high adverse gradients. The latter would probably be amplified into even higher gradients of velocity on the blade suction surface. The S9D design best illustrates the desirable features. They resulted from small incidence angles, relatively low inlet segment turning rates, and transition at about one-third chord. However, adequate choke margins and best throat locations may modify some of these choices, made mainly on the basis of expected boundary-layer behavior. This will be discussed later.

The effects of different weight flows on the meridional distribution of midchannel velocities for the same three stators and five spanwise locations are shown in figure 2. The three actual operating flows shown are those at wide-open throttle (maximum flow), near peak stage efficiency, and near stage stall (minimum flow). The design distributions of midchannel velocities are repeated from the previous figure for reference. The shift in midchannel velocity levels with flow is apparent and similar for the three designs. The local velocity gradients with the varying weight flows tend to reflect the design trends with some exceptions at maximum flow. At the maximum flow conditions the maximum midchannel velocities are near 325 meters per second in the hub region, just under sonic values.

Another way of viewing the midchannel velocity results for a particular blade design and operating point is by a velocity contours plot on the entire hub-to-shroud meridional plane. A typical one is shown in figure 3 for S9D operating near peak efficiency. (This

operating point was also used in the previous figure.) The midchannel velocity contours give a graphic sense of the flow through the blade row. It is apparent from such a plot that more critical flow regions are near the hub. There, velocity levels are highest and the meridional gradients are steeper.

The MERIDL code calculates midchannel velocities along the end-walls as well as at the other selected spanwise locations. These end-wall distributions may prove useful in understanding or correlating end-wall loss and in predicting wall stall. As shown in Part I (ref. 1), the stator hub region initiated stage stall at design speed for S9, S9R, S9C, and S9D. Attempts to identify some critical aspect of the calculated hub-wall velocity gradients with stall have produced inconclusive results. Verification data on actual wall gradients and further study are needed. Perhaps some combination of wall and blade-surface gradients in the hub region is necessary, along with some measure of the oncoming wall boundary layer.

Streamtube heights. - The meridional distribution of stream-tube height is an output of the MERIDL calculation. It is also a required input to the TSONIC calculation. These heights are shown in figure 4 as ratios to the blade span at the stator leading edge. The heights are based on passing 1 percent of the total flow of one blade-to-blade passage. An absolute value of 0.01 and constant chordwise and spanwise would be expected for ideal, incompressible flow in an infinite, two-dimensional cascade. Stream-tube height-to-span ratios are linear in the meridional direction and are nearly constant at midspan over a wide range of flows for the different designs studied. They are lower near the tip and higher near the hub because of their inverse relation with blade spacing, which depends on radius.

It should be noted that relatively small changes in stream-tube height result in relatively large changes in flow Mach number as sonic flow is approached. For example, if the inlet flow Mach number were 0.85 (typical for stator hubs herein) and the flow area were reduced 1 percent, the Mach number would increase to about 0.895. Blade surface velocities would also respond disproportionately to such a change in flow area at these inlet Mach number levels.

Analytical results versus data. - As previously indicated, the upstream and downstream radial distributions of total pressures and temperatures (upstream only) and tangential components of velocity are required inputs to the MERIDL calculation. Even though these boundary values are taken directly from measurements, MERIDL calculates somewhat different stream velocities than does the data reduction process. Some examples of this are shown in figure 5 where velocities at the upstream and downstream measuring stations are compared.

At the upstream station both the absolute velocity and its meridional component are shown. At the downstream station these are essentially the same because of the near-axial flow at the stator outlet. The three parts of the figure are for the three stator designs, each operating near peak stage efficiency at design speed. Generally, the veloc-

ities from the data-reduction program are slightly higher than those calculated from MERIDL over most of the span. Also, a flow calculation can be made by integrating the product of the locally measured velocity (meridional component), density, and flow area across the radius at any measuring station. This provides flow values that are generally somewhat higher than the total flow measured by the orifice which is used as MERIDL input. Evidence of these total-flow differences can be seen in the overall performance data in Part I (ref. 1, tables X to XIII), where the integrated flow at each measuring station is given along with the orifice value. These differences in velocity and flow are always less than 10 percent and are attributed to unaccounted for blockage effects in MERIDL and in the data reduction codes.

Inviscid Flow Calculations - Blade-To-Blade Solutions

Surface velocities from TSONIC. - The design values of these velocities are plotted as functions of meridional distance (or percent chord) from the leading edge in figure 6. Stator designs and spanwise locations are the same as for figure 1. Also, midchannel velocities, blade-section centerline turning rates, inlet- and outlet-segment cambers, transition locations, incidence angles, and leading- and trailing-edge velocities are repeated from figure 1 for convenience.

The maximum surface velocity is always on the suction side. When its value from TSONIC is changing rapidly near the leading edge (like S9 at 90 percent span from tip), it is difficult to calculate a reliable absolute value. In these cases a consistent, if somewhat arbitrary, approach was used, which took the suction-surface velocity at 2.5 percent chord to represent the maximum value. This location is typically about the closest to the leading edge that surface taps and thus experimental data are possible in conventional cascade tests. The ratio of the maximum suction-surface velocity to an axisymmetric average (blade-to-blade) of the flow velocity at the trailing edge, $V_{\max, ss}/V_{TE}$, is shown in figure 6 and will be discussed later.

The influence of blade design parameters such as incidence angle, inlet- to outlet-segment turning-rate ratios, and their transition locations on midchannel velocity distributions was discussed with figure 1. There, the expectation of similar effects on blade-surface velocities was indicated. Some major effects of these design parameters on surface-velocity distributions can be seen in figure 6. Because these design parameters are generally optional, they can be selected to control the velocity distributions.

The effect of a relatively high incidence angle is to increase the value of $V_{\max, ss}$ and move it closer to the leading edge. A comparison of either S9 or S9C with S9D, near the tip, shows this. Blade loading (as indicated by the difference in velocities between suction and pressure surface) also shifts forward. As will be shown later, the

higher incidence-angle designs generally resulted in higher losses and reduced stable operating ranges.

An effect of inlet- to outlet-segment turning-rate ratio, coupled with a change in transition location, is to shift the chordwise distribution of loading. For turning-rate ratios greater than unity along with transitions near 20-percent chord, like S9C, blade loading is mostly forward. For comparison, S9D turning rates are less than one, transitions are near 30 percent chord, and loading is toward the rear (see 70 percent span where S9C and S9D incidence angles are nearly equal). Some improvement in stable operating range will be subsequently shown for the more rear loaded designs. The importance of controlling chordwise loading distribution for optimized blade shapes should increase as even more is learned about its effect in both two- and three-dimensional flow regions of the blade.

An effect of a large change in turning-rate ratio from a value greater than one is to locally relax the adverse gradient on the suction surface as shown by S9C. Such control could prove useful in relieving a rapidly thickening boundary layer, thereby delaying its separation.

There is no intent here to specify a best design. Rather, it is to show how these analysis codes can be used to guide and optimize the selection of blade design parameters in order to obtain the most favorable surface-velocity distributions for a given application. The effects of other design options like solidity and chord length need to be studied over wider ranges than done here. Also, the importance of the surface-velocity distribution on and near the leading-edge circle needs to be evaluated.

The chordwise distributions of surface and midchannel velocities for all stators tested are shown in figures 7 to 10 for three operating points at design speed. These operating points were for weight flows near stage stall, near peak stage efficiency, and at wide-open throttle. Two intermediate weight flows (near peak stage efficiency) are shown for S9R. Measured blade-element losses and incidence angles are also given.

Near peak efficiency operation, the S9D surface-velocity distributions (fig. 10) resulted in the lowest $V_{\max,ss}/V_{TE}$ ratios and the lowest loss levels in the 30- to 70-percent midspan region. Also, the location of $V_{\max,ss}$ was near the leading edge. Here, the incidence angles were near zero; inlet- to outlet-segment turning-rate ratios were less than one; and transition was near one-third chord, as previously discussed (fig. 6). Thus, the milder surface velocity peaks and gradients for S9D that were first indicated by the midchannel calculations from MERIDL (fig. 1) have produced the lowest losses in the midspan region. However, in both end-wall regions (10- and 90-percent span) the story is different. Here, the shorter chord S9 (fig. 7), or S9R (fig. 8), blade exhibits the lowest loss even though they exhibit the highest suction-surface velocity gradients. As indicated in Part I perhaps the secondary flows or corner vortices are weaker with the shorter chord due to the shorter time to develop. Such three-dimensional effects cannot be predicted by the present analysis codes.

For off-design operation between peak efficiency and near stall (figs. 7 to 10), there is a consistent pattern: The blade loading shifts toward the leading edge as the incidence angle increases. This in turn increases $V_{\max,ss}/V_{TE}$ and the level of measured loss. The slowest increase of $V_{\max,ss}/V_{TE}$ was with the S9D design. It also exhibited the lowest stall flow of all those studied (as shown in Part I). These characteristics may be related to the MCA segment turning-rate ratio (fig. 6). For the S9D design, the ratio was less than one.

Because it was determined that stage stall at design speed was controlled by the flow in the stator hub region (refs. 1 and 2), some attempts have been made to relate these stalls to the velocity gradients on the blade surface as calculated by TSONIC. As previously discussed, similar attempts were made using the hub-wall velocity gradients calculated by MERIDL. Some simple combinations of wall and blade have also been tried. These approaches have been inconclusive to date. Analysis-code predictions of blade-row stall are highly desirable, of course, and will continue to be sought.

Turning to wide-open throttle operation, the velocity distributions are generally different in shape and level than those at the lower flows. At maximum flow $V_{\max,ss}$ is no longer a sharp peak near the leading edge. Instead, it may be nearly a plateau over a third or more of the chord (see midspan S9 or S9C, figs. 7(c) or 9(c) or a well defined peak that is near midchord (see midspan S9D, fig. 10(c)). Thus, most of the suction-surface diffusion is over a shorter distance. This could result in earlier boundary layer separation and higher loss. There may also be choked flow effects at wide-open throttle points that increase losses in ways not obvious from just surface-velocity distributions or levels of surface Mach numbers.

The wide-open throttle operation of S9D (fig. 10(c)) indicates a potential problem with having relatively low inlet segment turning rates. These, combined with a more rearward transition location and low incidence angle, produced flow area minimums at design that are relatively small and well inside the covered passage. As shown in figure 4(i) of Part I the minimum flow areas in terms of choke margins for each blade element of the S9, S9C, and S9D designs vary. Over the inner half span, S9D had by far the lowest design choke margin. It was about 2 percent near the hub, and the throat occurred well inside the covered passage. In contrast, for the wide-open throttle operation of S9C (fig. 9(c)) over the inner half span, $V_{\max,ss}$ remains much nearer the leading edge. This is due to the higher inlet segment turning rates and the more forward transition location of the S9C design (see fig. 6(b)). The resulting losses for S9C are also lower than for S9D at the wide-open throttle condition.

Finally, about the wide-open throttle data near the hub (figs. 7 to 10), the velocity distributions for all stators studied are indicated with broken lines. Choked flow is also noted over a narrow region near the leading edge. The quality of these TSONIC solutions is reduced because they required a small reduction in the actual weight flow locally (generally less than 2 percent) to obtain a converged solution.

So far, only 100-percent speed cases have been discussed. As shown in Part I (figs. 13 to 16), the operating flow range of these stators is more than doubled at 70 compared with 100 percent of design speed. How these wider flow ranges at part speed affect the chordwise distribution of surface velocities at 50-percent span for S9, S9C, and S9D are shown in figure 11. For S9, the incidence angle ranged from 0.5° at wide-open throttle to 22.5° at near-stall operation. Along with this, $V_{\max,ss}/V_{TE}$ ranged from 1.54 to 2.12. For S9C and S9D at wide-open throttle operation, negative incidence angles occurred. For these cases, $V_{\max,ss}$ was located near 45 percent chord. For S9D an incidence angle of -3.1° was near the peak stage efficiency operation at 70 percent speed.

These part-speed results illustrate the large changes in surface-velocity distributions that can occur over operating ranges of interest.

From these observations made from figures 6 to 11, a brief summary of blade-design features believed to produce desirable blade-surface velocity distributions and thus good performance for MCA stators with inlet Mach numbers and solidities like those studied is as follows: (1) blade-element values of $V_{\max,ss}/V_{TE}$ should be minimized, and $V_{\max,ss}$ should be near the leading edge; (2) incidence angles near zero, inlet-to outlet-segment turning rate ratios less than one, and thin blades and edges all help to achieve item (1); (3) in minimizing $V_{\max,ss}/V_{TE}$ adequate choke margins should be retained and the blade-element throats should be at the start of the covered passage; and (4) in both end-wall regions, a short chord seemed to be more relevant to minimizing losses than blade-surface velocity distributions.

Surface velocities - comparison of calculation methods. - As previously indicated, the MERIDL analysis also estimates blade-surface velocities. The accuracy of these velocities is not as good as those from TSONIC because of the additional simplifying assumptions involved (refs. 7 and 8). However, for each operating point, one MERIDL solution simultaneously provides surface-velocity distributions for all the different streamlines selected for analysis. In contrast, one TSONIC solution provides surface velocities for only one streamline or stream surface. Thus, it is of interest to know the relative quality of these calculations. Such a comparison is shown in figure 12 for S9 and in figure 13 for S9D.

The general character of the surface-velocity distributions from MERIDL are similar to those from TSONIC. However, some of the $V_{\max,ss}$ values and their chordwise locations differ, as do local gradients of velocity. The results suggest that MERIDL solutions for blade-element surface velocities may be sufficiently accurate for preliminary design or analysis. But for final evaluations, a series of TSONIC solutions for different streamline locations across the span are recommended.

Loss Correlations

Background. - After the development of the diffusion factor

$$D = \frac{V_{\max, ss}}{V_{LE}} - \frac{V_{TE}}{V_{LE}}$$

and its use in correlating incompressible, two-dimensional blade losses in cascade (ref. 10), a more basic analysis, corroborated by several sets of cascade data, was proposed by Lieblein in reference 11. There, starting from basic boundary-layer theory, the ratio of the wake momentum thickness at the blade trailing edge at minimum loss incidence angle to chord θ_{TE}^*/C was shown to be a function of the magnitude of velocity diffusion on the suction surface. This diffusion was expressed as the ratio of maximum suction-surface velocity $V_{\max, ss}$ to trailing-edge velocity V_{TE} . This suction-surface diffusion ratio is also known as D_{eq} , for equivalent diffusion; where

$$D_{eq} = \frac{V_{\max, ss}}{V_{TE}}$$

The location of $V_{\max, ss}$ was at or near the blade leading edge, and the value of V_{TE} was from measurements of the average (blade-to-blade) velocity at the blade outlet measuring station.

In a previous theoretical analysis of minimum-loss relations in low-speed cascade flow, Lieblein and Roudebush (ref. 12) showed that the total-loss parameter $\bar{\omega} \cos \beta_{TE}/2\sigma$ was proportional to θ_{TE}^*/C . Thus, correlations of blade minimum total-loss parameters ($\bar{\omega} \cos \beta_{TE}/2\sigma$ or $\bar{\omega}_w \cos \beta_{TE}/2\sigma$) with D_{eq} or with D-factor have had a successful history. Therefore, it was logical to try similar loss correlations in the present study, but with the values of V_{LE} , V_{TE} , and $V_{\max, ss}$ calculated from the internal flow-analysis codes. Usually these values are measured (V_{LE} and V_{TE}) or estimated ($V_{\max, ss}$) from velocity diagram data at blade inlet and outlet. An estimate of $V_{\max, ss}$ from the D-factor development of reference 10 is often expressed as

$$\frac{V_{\max, ss}}{V_{LE}} = 1 + \left| \frac{(rV_{\theta})_{TE} - (rV_{\theta})_{LE}}{(r_{LE} + r_{TE})\sigma V_{LE}} \right| \quad (1)$$

from which is obtained

$$\frac{V_{\max, ss}}{V_{TE}} = \left[1 + \left| \frac{(rV_{\theta})_{TE} - (rV_{\theta})_{LE}}{(r_{LE} + r_{TE})\sigma V_{LE}} \right| \right] \left(\frac{V_{LE}}{V_{TE}} \right) = D_{eq} \quad (2)$$

Results of loss correlations using internal-flow analysis calculations and comparisons with those using velocity-diagram estimates are presented in the following sections.

Using velocities from internal-flow analysis calculations. - The measured stator wake total-loss parameter ($\bar{\omega}_w \cos \beta_{TE}/2\sigma$) is presented as a function of the suction-surface diffusion ratio $V_{\max, ss}/V_{TE}$ in figure 14. All operating conditions, stator designs, and spanwise locations studied are shown. The plots indicate that, over most of the blade span and operating range, $V_{\max, ss}/V_{TE}$ is the primary variable governing blade-element loss. In the midspan region (30 to 70 percent span) $V_{\max, ss}/V_{TE}$ increases as flow is reduced from minimum loss toward near-stall operation for all designs. Reasons for this were previously discussed (with figs. 7 to 11). As $V_{\max, ss}/V_{TE}$ increases so do the losses, and a common curve correlates them for the different stators and speeds. This occurs even though the blade designs, incidence angles, and surface-velocity gradients are quite different, as previously illustrated. In this midspan region and for the blade designs and flows from minimum loss to near stall studied at design speed, the moderate chord length designs (S9C and S9D) exhibited generally lower values of $V_{\max, ss}/V_{TE}$ and thus loss than did the short-chord design (S9, S9R). This result is due to the lower incidence angles, smaller leading-edge thickness to chord ratios, and smaller maximum-thickness-to-chord ratios (see ref. 1, fig. 4). If the present short-chord design was modified in these directions, it should operate at reduced loss. An example of such a redesign is presented in a subsequent section.

There are some departures from the correlation curves shown (fig. 14). One is for the tailed data points from wide-open throttle operation at design speed. Here losses are high, even though $V_{\max, ss}/V_{TE}$ is relatively low. At these high flows there tend to be relatively large velocity decelerations on both suction and pressure surfaces, as previously discussed (figs. 7(d) to 10(d)). There may also be additional losses related to choking that are not understood or obvious from the surface-velocity distributions. The other departure from the curves drawn is the increased data scatter at $V_{\max, ss}/V_{TE}$ values above about 1.9. Near-stall flows with high incidence angles are generally associated with these levels of $V_{\max, ss}/V_{TE}$ (figs. 7(a) to 10(a) and 11). This results in large local decelerations on the suction surface near the leading edge, which in turn probably causes earlier boundary-layer separation and increased loss. Such flow conditions are likely to result in more erratic boundary-layer behavior and make accurate loss prediction more difficult. Similar increases in loss data scatter were noted in reference 11 when $V_{\max, ss}/V_{TE}$ values became greater than 1.9.

In the end-wall regions (10- and 90-percent span, fig. 14) there is not the same loss correlation with $V_{\max, ss}/V_{TE}$ as for midspan, and loss levels are generally higher. Also, near the hub, losses are independent of $V_{\max, ss}/V_{TE}$. Here, other effects, probably three dimensional, are influencing loss that are not sensitive to the two-dimensional $V_{\max, ss}/V_{TE}$ parameter. End-wall, minimum-loss levels are about

three times the midspan values for S9C and S9D (moderate chord) and about twice the midspan values for S9 and S9R (short chord). Reduced, secondary flows with weaker corner vortices with the shorter chord are possible reasons for these end-wall loss comparisons. Whether this short-chord advantage applies to loading levels and degrees of exit swirl other than those studied is not presently known.

Discussions thus far have shown promising loss correlations with a suction-surface diffusion ratio $V_{\max, ss}/V_{TE}$, evaluated by internal-flow analysis where the local velocities are calculated directly. However, with conventional design and off-design prediction methods and data-reduction codes, suction-surface diffusion is determined from the velocity diagrams at the blade inlet and outlet. In the following discussion, loss correlations with each source of $V_{\max, ss}/V_{TE}$ are evaluated and compared. The midspan region (30 to 70 percent) data and the flow range from minimum loss to near stall will be the basis for this discussion.

Using velocities from diagrams at blade inlet and outlet and comparisons with internal-flow analysis. - D_{eq} and D are different combinations of the velocity ratios $V_{\max, ss}/V_{TE}$ and V_{TE}/V_{LE} and are related as follows:

$$D_{eq} = \frac{V_{\max, ss}}{V_{LE}} \div \frac{V_{TE}}{V_{LE}} = \frac{V_{\max, ss}}{V_{TE}} \quad (3)$$

$$D = \frac{V_{\max, ss}}{V_{LE}} - \frac{V_{TE}}{V_{LE}} \quad (4)$$

$$D = (D_{eq} - 1) \frac{V_{TE}}{V_{LE}} \quad (5)$$

Minimum loss as a function of $V_{\max, ss}/V_{LE}$ and V_{TE}/V_{LE} is shown in figure 15. In part (a) the velocities are from internal-flow analysis, and in part (b) they are from velocity-diagram data at blade inlet and outlet. (Note that $V_{\max, ss}/V_{LE}$ from the velocity-diagram data was defined previously, eq. (1).) The two velocity ratios are shown separately to indicate how each responds to changes in blade geometry and flow and not to imply a better loss correlating term than the established groupings just reviewed. The values of V_{TE}/V_{LE} are about the same in comparing parts (a) and (b), but the values of $V_{\max, ss}/V_{LE}$ are not. According to internal-flow analysis, $V_{\max, ss}/V_{LE}$ varies from about 1.1 to 1.35, whereas estimates from the velocity diagrams give a nearly constant value of 1.15. A slightly different velocity-diagram estimate (not shown here) developed in reference 11 for C.4 circular-arc and NASA 65(A₁₀) blades gives a little higher but also nearly constant value of $V_{\max, ss}/V_{LE}$ of 1.26.

The highest values of $V_{\max, ss}/V_{LE}$ (fig. 15(a)) are for S9 and S9R. Thus the highest values of $V_{\max, ss}/V_{TE}$ are also for S9 and S9R, as shown in figure 16. There, internal-flow analysis values are in part (a), and velocity-diagram values are in part (b). Stators 9 and 9R operated at relatively high incidence angles even at minimum loss (figs. 7(b) and 8(b)). Whereas the analysis codes responded as expected with noticeably higher $V_{\max, ss}/V_{LE}$ values at the higher incidence angles, the velocity-diagram estimates did not. This is shown in figure 17 where $V_{\max, ss}/V_{LE}$ is presented as a function of incidence angle for the same minimum-loss data as in figures 15 and 16. As before, parts (a) and (b) segregate the velocity sources.

The incidence-angle dependence for angles greater than zero (fig. 17) is about seven times larger using the analysis codes compared with the velocity-diagram estimates as shown by the equations in the figure. There is some response to incidence angle in the velocity-diagram estimates, but it is small. It is recognized that the $V_{\max, ss}/V_{LE}$ values from internal-flow analysis respond to camber and thickness changes as well as to incidence angle. Perhaps relatively high front camber or high front turning rates act like increased incidence. However, the higher incidence angles (above zero) are believed mainly responsible for the increased $V_{\max, ss}/V_{LE}$ and, thus, loss with the present data. Note the S9C and S9D levels of $V_{\max, ss}/V_{LE}$ in figure 17(a) near a common value of incidence of 3° ; these levels are about the same even though their front cambers (and front turning rates) are much different (see fig. 6).

In summary, the minimum-loss data of figures 15 to 17 indicate that, for the range of blade geometries and flow conditions studied here, incidence angles (i_{mc}) near zero provided the lowest losses over the midspan region.

Loss data between minimum-loss and near-stall operation are added to the minimum-loss data of figures 15 and 17 and presented in figures 18 and 19. The effect of the higher incidence angles near stall on $V_{\max, ss}/V_{LE}$ is evident from the internal-flow analysis calculations. In contrast, the velocity-diagram estimates are little changed by increased incidence. The $V_{\max, ss}/V_{LE}$ relations with incidence angle are the same as at minimum-loss operation.

The loss data at minimum-loss to near-stall operation as a function of $V_{\max, ss}/V_{TE}$ are shown in figure 20. There is little correlation of loss with D_{eq} (fig. 20(b)) for the higher-incidence-angle, off-design operation. In contrast, a reasonably good correlation is obtained by the internal-flow analysis calculation (fig. 20(a)). More importantly, the latter provides a realistic value of the magnitude of velocity diffusion on the suction surface, which in turn relates directly to loss over a wide range of flows. The correlation curve drawn in figure 20(a) is the same as that previously shown for the midspan region in figure 14. It is also an extension of the minimum-loss curve of figure 16(a) to higher values of $V_{\max, ss}/V_{TE}$.

Estimating blade maximum suction-surface velocity at off-design operation. - Instead of using calculated surface velocities from internal-flow analysis codes to corre-

late off-design losses, the D_{eq} parameter might be modified with additional, but readily available, terms to better approximate the value of $V_{max, ss}/V_{LE}$. Such an approach was used by Lieblein in reference 11. There, an incidence-angle term was added to a minimum-loss, D_{eq} correlation. The additive term was an incidence-angle difference from minimum loss raised to a power.

As previously indicated by figure 19, a much improved estimated of $V_{max, ss}/V_{LE}$ for the present data could be obtained over a wide range of positive incidence angles if an incidence angle correction is made to the velocity-diagram prediction. This correction is $0.92 (i_{mc})_{rad}$, the difference in the $V_{max, ss}/V_{LE}$ expressions shown in figures 19(a) and (b). Thus

$$\frac{V_{max, ss}}{V_{TE}} = \left[1 + \frac{(rV_{\theta})_{TE} - (rV_{\theta})_{LE}}{(r_{LE} + r_{TE})\sigma V_{LE}} \right] + 0.92 (i_{mc})_{rad} \left(\frac{V_{LE}}{V_{TE}} \right) \quad (6)$$

The improved off-design loss correlation with this incidence angle term added is illustrated in figure 21(a). Figure 21(b) repeats fig. 20(b) to conveniently illustrate the improvement. Although the correlation curve drawn in figure 21(a) is somewhat different from the one drawn for the analysis code values in figure 20(a), the data scatter from each is comparable.

It is recognized that, for stator-blade shapes and solidities much different from those studied, minimum loss may not occur near zero incidence angle. To allow for such possibilities, the incidence-angle correction could just as easily be in the form of a constant times an incidence-angle difference from the value at minimum loss. For the present data the value at minimum loss happens to be zero. Also, as in reference 11, the constant may be related to the blade shape.

A comparison of correlations for the effect of off-design incidence angle on the maximum suction-surface to leading-edge velocity ratio increment above minimum-loss levels is shown in figure 22. The two relations suggested by the data of reference 11 (for C.4 circular-arc and NACA 65(A₁₀) blades in low speed, linear cascades) are plotted along with the present correction obtained for the midspan region of multiple-circular-arc (MCA) blades operating behind a transonic rotor. For incidence angles from 0 to about 12° the circular-arc cascade correction fits the present data just as well as the one developed here. Above 12° incidence the exponential relation of reference 11 for the circular-arc blades increasingly deviates from the present data. The exponential relation for the NACA 65(A₁₀) blades falls increasingly above the present data as incidence angle increases above 0.

In summary, with a simple incidence-angle correction term a realistic estimate of the suction-surface diffusion ratio was possible from velocity-diagram data obtained at the inlet and outlet of the blade shapes studied over a wide range of flows from minimum

loss to near stall. This in turn allowed a good correlation of loss over the midspan region. The improved velocity-diagram estimate of suction-surface diffusion should be most useful for off-design loss predictions where incidence angles are generally greater than zero.

Using Analysis Codes in Design

The loss correlations of figure 14 show a direct relation between $\bar{\omega}_w$ and $V_{\max,ss}/V_{TE}$. Because V_{TE} is essentially fixed by the overall requirements of an axisymmetric aerodynamic design, a reduction in $V_{\max,ss}$ will reduce $\bar{\omega}_w$. The inviscid internal-flow-analysis codes are effective tools for studying the influence of many of the various blade design options, like incidence angle and camber and thickness distributions, on the value of $V_{\max,ss}$. They can be used to seek optimum combinations for minimum $V_{\max,ss}$ and thus minimum $\bar{\omega}_w$. This is not possible with the conventional D_{eq} or D-factor approach.

The present approach is believed generally applicable in a design procedure, although it does not resolve all the design options like optimum chord length or solidity. Also, the absolute values of loss involved are limited to the class of blade geometries that have been tested, analyzed, and correlated with $V_{\max,ss}/V_{TE}$.

To illustrate the use of MERIDL and TSONIC in a design procedure and the potential benefits therefrom, stator 9 has been redesigned. The original blade number and solidity (thus chord length) were unchanged. Reasons for these selections are as follows: (1) Noise benefits from use of stator-to-rotor blade number ratios greater than about two are being verified in flight tests (ref. 13). For operation with the 53 rotor blades of rotor 15 in the NASA QF-1 design, about 112 short-chord stators are required. (2) Short-chord designs are of interest for applications where minimum axial length of the machine is critical, as for a fan-in-wing, VTOL aircraft. (3) The short-chord S9 design has shown lower three-dimensional losses in both end-wall regions than the moderate-chord S9C and S9D designs. (4) Keeping the same solidity also assures the applicability of the absolute values of the present loss correlation. The value of $V_{\max,ss}$ is sensitive to solidity levels, and these varied, at the tip, only from 1.4 to 1.5 in the present study (ref. 1).

If the blade-element losses could be reduced by analysis-code-guided selection of blade-design options, the overall loss of this redesigned, short-chord stator, to be called S9H, could make it competitive with the best known, moderate chord, high-inlet-Mach-number, MCA stator, which is S9D. The inlet conditions for S9H were those measured behind rotor 15 at its peak efficiency operation. And air turning to the axial direction at the outlet of S9H was specified.

The radial distributions of incidence angles and blade geometry finally selected for S9H are presented and compared with S9 in figure 23. The MCA geometry variables explored included inlet-to-outlet-segment turning rate ratio, location of transition, maximum thickness and its location, and leading-edge thickness. Many combinations of these blade design options were studied in an effort to find the optimum. Also, for the same inlet air angle, incidence-angle-versus-inlet-mean-line-metal-angle trade studies were made with the most promising combinations.

There was a large change in incidence angle i_{mc} between S9 and S9H with an S9H value of zero (fig. 23(a)). There was a corresponding increase in inlet mean line metal angle $(\kappa_{mc})_{LE}$ (fig. 23(k)). A reduced maximum thickness (fig. 23(d)) was possible for S9H because of its increased camber and also because it could be machined rather than cast (see ref. 1, table V footnote). The leading- and trailing-edge thicknesses (fig. 23(e)) were reduced to the machineable minimum of 0.0254 centimeter (0.010 in.).

The choke margin (fig. 23(i)) in the hub region of S9H is considerably less than that for S9. However, a minimum value of 3 percent at about 75 percent span, along with a spanwise average of about 6 percent, is considered adequate. To achieve this choke margin, the location of maximum thickness (fig. 23(j)) was moved rearward to 65 percent chord at the hub. The transition location distribution (fig. 23(g)) was the result of moving the maximum thickness rearward, and also of requiring a continually decreasing blade thickness from maximum to either the leading or trailing edge.

A comparison of blade shapes between S9 and S9H is shown in figure 24. Three spanwise locations (10, 50, and 90 percent) are shown as well as the inlet and outlet turning rates, transition locations, and cambers. The increase in inlet camber and reduction in blade thickness are the major changes for S9H. Moving the transition location from about 20 to 40 percent chord was a bigger factor in increasing inlet camber than was inlet turning rate. Inlet turning rate was also increased except at the hub.

Surface-velocity distributions for S9H at five spanwise locations are compared with those for S9 in figure 25. For S9 both the design distributions and those while operating at near-peak stage efficiency (ref. 2, data reading 601) are shown. Values of $V_{max,ss}/V_{TE}$ and $M_{max,ss}$ are also tabulated. For all spanwise sections, the diffusion ratio $V_{max,ss}/V_{TE}$ for the redesigned S9H is lower than for S9 at peak stage operation. And S9H diffusion ratios are much lower than those now predictable for the original S9 design. The midspan $V_{max,ss}/V_{TE}$ of 1.60 for S9H compares with 1.74 for S9 and 1.59 for S9D (see fig. 10(b)) both at peak operation. Nearest the hub, $M_{max,ss}$ has been reduced from 1.3 to 1.135 (S9 to S9H). Also, the location of the peak suction-surface velocity is usually near the leading edge. This location is assumed or known in the development of the D-factor and D_{eq} correlations (refs. 10 and 11). Peak suction-surface velocities near the leading edge are also part of the present loss

correlations. That location for the peak also indicates that minimum-flow areas in a blade-to-blade plane are at, or near, the start of the covered passage. This is believed to be the best location.

Although $V_{\max, ss}/V_{TE}$ values are lower for S9H than S9, the pressure surface velocity diffusions are higher for S9H, particularly near the hub. Boundary layer calculations were made with the S9H pressure surface gradients, and turbulent separation was not indicated for the design conditions. Such pressure surface performance is not expected to have a major adverse effect on the overall performance of S9H compared with S9. The reduced $V_{\max, ss}/V_{TE}$ ratios for S9H compared with S9 result in reduced $\bar{\omega}_w$ from the figure 14 correlation. These loss coefficients and accompanying stage efficiencies are shown in figure 26. In terms of an overall increase in stage efficiency (mass averaged), a gain of 1.6 points is predicted for S9H compared with the peak previously measured with S9.

As shown in figure 18(b) of Part I the efficiency decrement for the peak performance of S9 was 5.7 points and that for S9D was 4.4 points. For S9H the decrement is estimated to be 4.1 points. This is for stator-inlet Mach numbers from about 0.7 to 0.9, a short chord of 1.86 centimeters (aspect ratio of 5.1), and D-factors of about 0.45.

CONCLUDING REMARKS

The present approach has shown that valuable insights on actual blade-row performance have been gained from internal-flow-analysis codes even though they were only inviscid and two dimensional. These codes begin to show how the flow parameters and details of the blade geometry interact to produce performance characteristics. This provides a system for optimizing the available design choices.

There remains of course a big difference between presently calculated, inviscid, two-dimensional flow and the real flow in a compressor. Thus efforts are continuing to improve the analysis codes through the inclusion of more real flow effects. The goal is to predict as many blade-row performance characteristics and levels as possible with the minimum reliance on data correlations.

SUMMARY OF RESULTS

A hub-to-shroud and a blade-to-blade flow analysis code, both inviscid and basically subsonic, were used to calculate flow parameters within four stator-blade rows. Some relations between these internal flow calculations and conventionally obtained performance results were established. A broad range of operating conditions were analyzed and the following principal results were obtained:

1. In the midspan region (30 to 70 percent span) the internal-flow-analysis-code calculated ratio of maximum-suction-surface velocity to trailing-edge velocity (suction-surface diffusion ratio) correlated the measured total-loss parameter over a wide range of flows from minimum-loss to near-stall operation and for all stators and speeds studied.

2. Adding a simple incidence-angle term to velocity diagram estimates of the suction-surface diffusion ratio improves its accuracy, which in turn provides a minimum-loss to near-stall loss correlation comparable to that obtained with the internal-flow analyses calculations.

3. The potential benefits of a blade designed with the aid of the present flow-analysis codes is illustrated by a proposed redesign of the original short-chord stator for NASA QF-1. For the same chord length and blade number, blade incidence angle and geometry were changed to minimize the maximum suction-surface velocity at each blade section. An overall efficiency improvement of 1.6 points above the peak previously measured with the original design is predicted for the redesign.

Lewis Research Center,
National Aeronautics and Space Administration,
Cleveland, Ohio, October 2, 1979,
505-04.

APPENDIX - SYMBOLS

D	diffusion factor, $1 - \frac{V'_{TE}}{V'_{LE}} + \left \frac{(rV_{\theta})_{TE} - (rV_{\theta})_{LE}}{(r_{TE} + r_{LE})\sigma(V')_{LE}} \right $; for stators,
	$D = 1 - \frac{V_{TE}}{V_{LE}} + \left \frac{(rV_{\theta})_{TE} - (rV_{\theta})_{LE}}{(r_{TE} + r_{LE})\sigma V_{LE}} \right $
D _{eq}	equivalent diffusion or suction-surface diffusion ratio, which for stator blades is $\frac{D}{V_{TE}/V_{LE}} + 1 = \frac{V_{max,ss}}{V_{TE}}$
i _{mc}	mean incidence angle, angle between inlet air direction and line tangent to blade mean camber line at leading edge, deg
i _{ss}	suction-surface incidence angle, angle between inlet air direction and line tangent to blade suction surface at leading edge, deg
M _{max,ss}	maximum Mach number on suction surface
P	total pressure
p	static pressure
r	radius
s	distance along blade surface
T	total temperature
V	air velocity
V _m	air velocity in meridional (radial-axial) plane
V _{max,ss}	maximum velocity on suction surface
V _θ	air velocity in tangential direction
w	weight flow, kg/sec
w _D	design weight flow, 29.16 kg/sec
β	air angle, angle between air velocity and axial direction, deg
γ	ratio of specific heats (1.40)
δ ⁰	deviation angle, angle between exit-air direction and tangent to blade mean camber line at trailing edge, deg

η_{ad} stage adiabatic (temperature-rise) efficiency, $\frac{(\overline{P_3/P_1})^{(\gamma-1)/\gamma} - 1}{(\overline{T_3/T_1}) - 1}$

κ_{mc} angle between blade mean camber line and meridional plane, deg

σ blade solidity, ratio of chord to spacing

$\overline{\omega}$ total-loss coefficient, $\frac{(P'_{id})_{TE} - \overline{P'}_{TE}}{P'_{LE} - p_{LE}} = \frac{P'_{LE} - \overline{P'}_{TE}}{P'_{LE} - p_{LE}}$

$\overline{\omega}_w$ wake total-loss coefficient, $\frac{(P'_{id})_{TE} - \overline{P'}_{TE}}{P'_{LE} - p_{LE}} = \frac{(P'_{TE})_{3hi\ a\ g} - \overline{P'}_{TE}}{P'_{LE} - p_{LE}}$

Subscripts:

id ideal

LE leading edge of blade

TE trailing edge of blade

1 instrumentation plane upstream of rotor (see ref. 1, fig. 1)

2a instrumentation plane near rotor trailing edge (see ref. 1, fig. 1)

2b instrumentation plane near stator leading edge (see ref. 1, fig. 1)

3 instrumentation plane downstream of stator (see ref. 1, fig. 1)

3hi a g average of three highest values of total pressure measured across stator gap at stator exit

Superscript:

' relative to blade

REFERENCES

1. Gelder, Thomas F.: Aerodynamic Performances of Three Fan Stator Designs Operating with Rotor Having Tip Speed of 337 Meters Per Second and Pressure Ratio of 1.54. I - Experimental Performance. NASA TP-1610, 1980.
2. Gelder, Thomas F.; and Lewis, George W., Jr.: Aerodynamic Performance of a 0.5-Meter-Diameter, 337-Meter-per-Second Tip Speed, 1.5-Pressure Ratio, Single-Stage Fan Designed for Low Noise Aircraft Engines. NASA TN D-7836, 1974.
3. Crouse, James E.: Computer Program for Definition of Transonic Axial-Flow Compressor Blade Rows. NASA TN D-7345, 1974.
4. Horlock, J. H.: Fluctuating Lift Forces on Airfoils Moving Through Transverse and Chordwise Gusts. J. Basic Eng., vol. 90, no. 4, Dec. 1968, pp. 494-500.
5. Dittmar, J. H.: Methods of Reducing Blade Passing Frequency Noise Generated by Rotor-Wake-Stator Interaction. NASA TM X-2669, 1972.
6. Harley, K. G.; Odegard, P. A.; and Burdsall, E. A.: High-Loading Low-Speed Fan Study. Part IV - Data and Performance with Redesign Stator and Including a Rotor Tip Casing Treatment. (PWA-4326, Pratt & Whitney Aircraft; NASA Contract NAS3-10483). NASA CR-120866, 1972.
7. Katsanis, Theodore; and McNally, William D.: Revised Fortran Program for Calculating Velocities, and Streamlines on the Hub-Shroud Midchannel Stream Surface of an Axial-, Radial-, or Mixed-Flow Turbomachine or Annular Duct. I: Users Manual. NASA TN D-8430, 1977.
8. Katsanis, Theodore: Fortran Program for Calculating Transonic Velocities on a Blade-to-Blade Stream Surface of a Turbomachine. NASA TN D-5427, 1969.
9. Sanger, Nelson L.: Two-Dimensional Analytical and Experimental Performance Comparison for a Compressor Stator Section with D-Factor of 0.47. NASA TN D-7425, 1973.
10. Lieblein, Seymour; Schwenk, Francis C.; and Broderick, Robert L.: Diffusion Factor for Estimating Losses and Limiting Blade Loadings in Axial-Flow-Compressor Blade Elements. NACA RM E53D01, 1953.
11. Lieblein, Seymour: Loss and Stall Analysis of Compressor Cascades. Trans. ASME, Series D, J. Basic Eng., vol. 81, no. 3, Sep. 1959, pp. 387-400.
12. Lieblein, Seymour; and Roudebush, William, H.: Theoretical Loss Relations for Low-Speed Two-Dimensional-Cascade Flow. NACA TN 3662, 1956.

13. Feiler, Charles E.; and Groeneweg, John F.: Summary of Forward Velocity Effects on Fan Noise. NASA TM-73722, 1977.

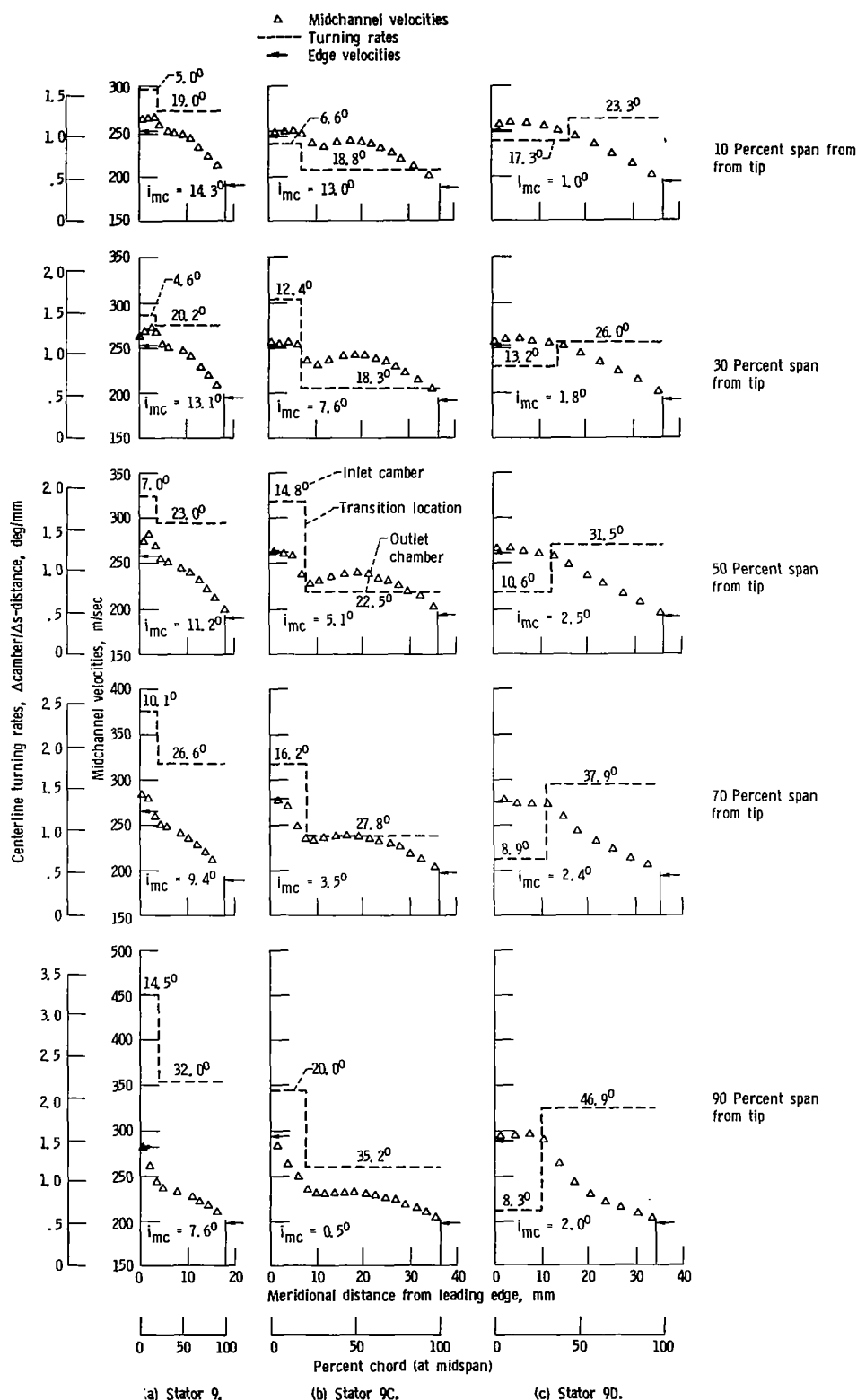


Figure 1. - Meridional distribution of midchannel velocities and blade section centerline turning rates for S9, S9C, and S9D at their design points.

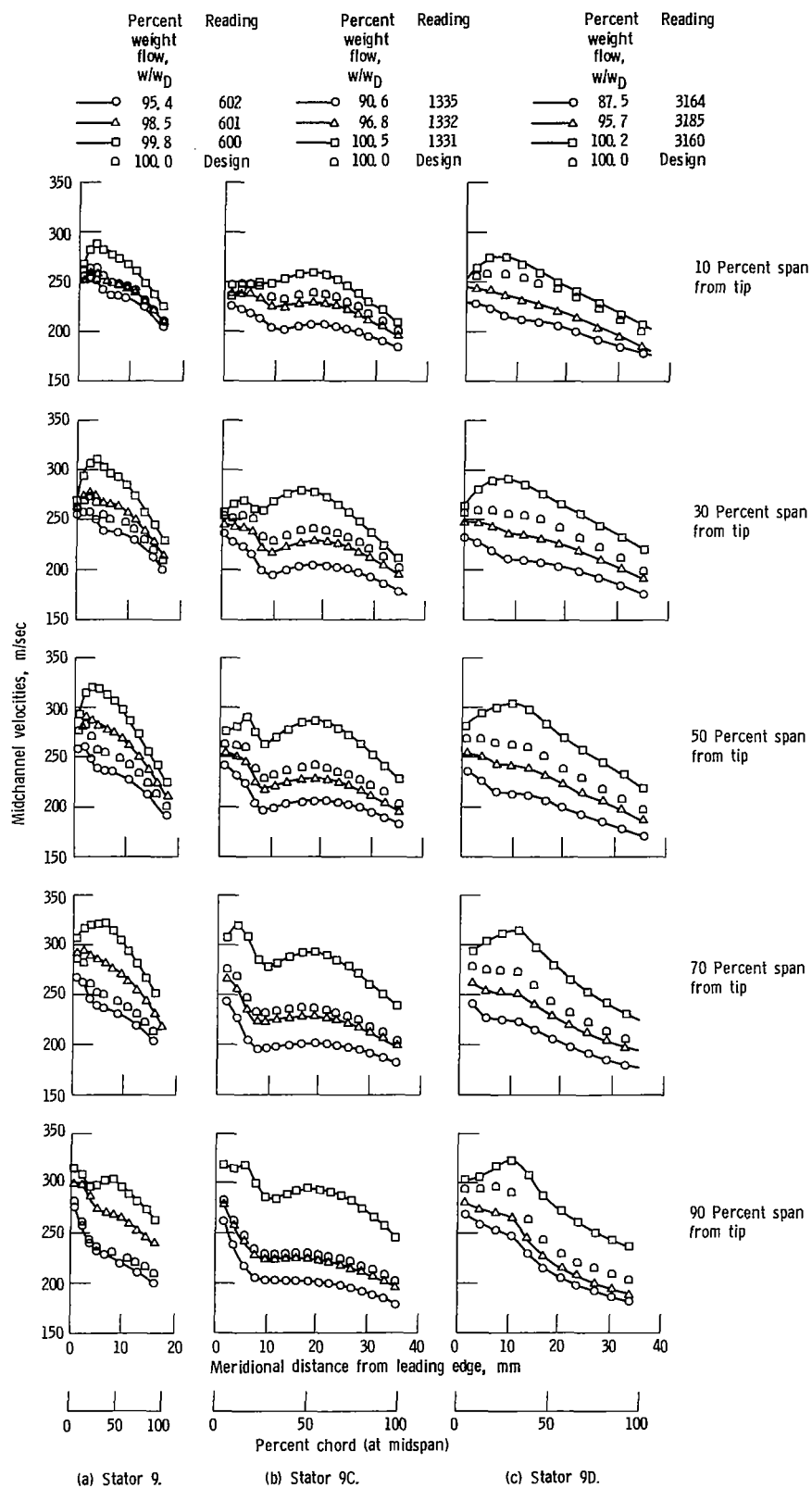


Figure 2. - Meridional distribution of midchannel velocities for S9, S9C, and S9D at three weight flows and at design speed.

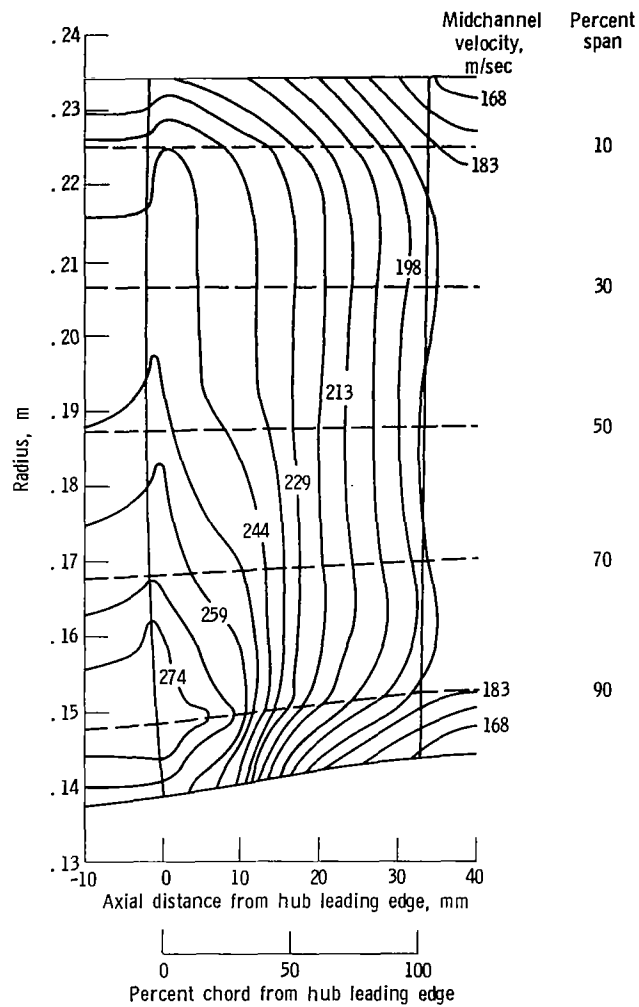


Figure 3. - Midchannel velocity contours for S9D at design speed and near-peak stage efficiency operation; 95.7 percent of design flow; reading 3185.

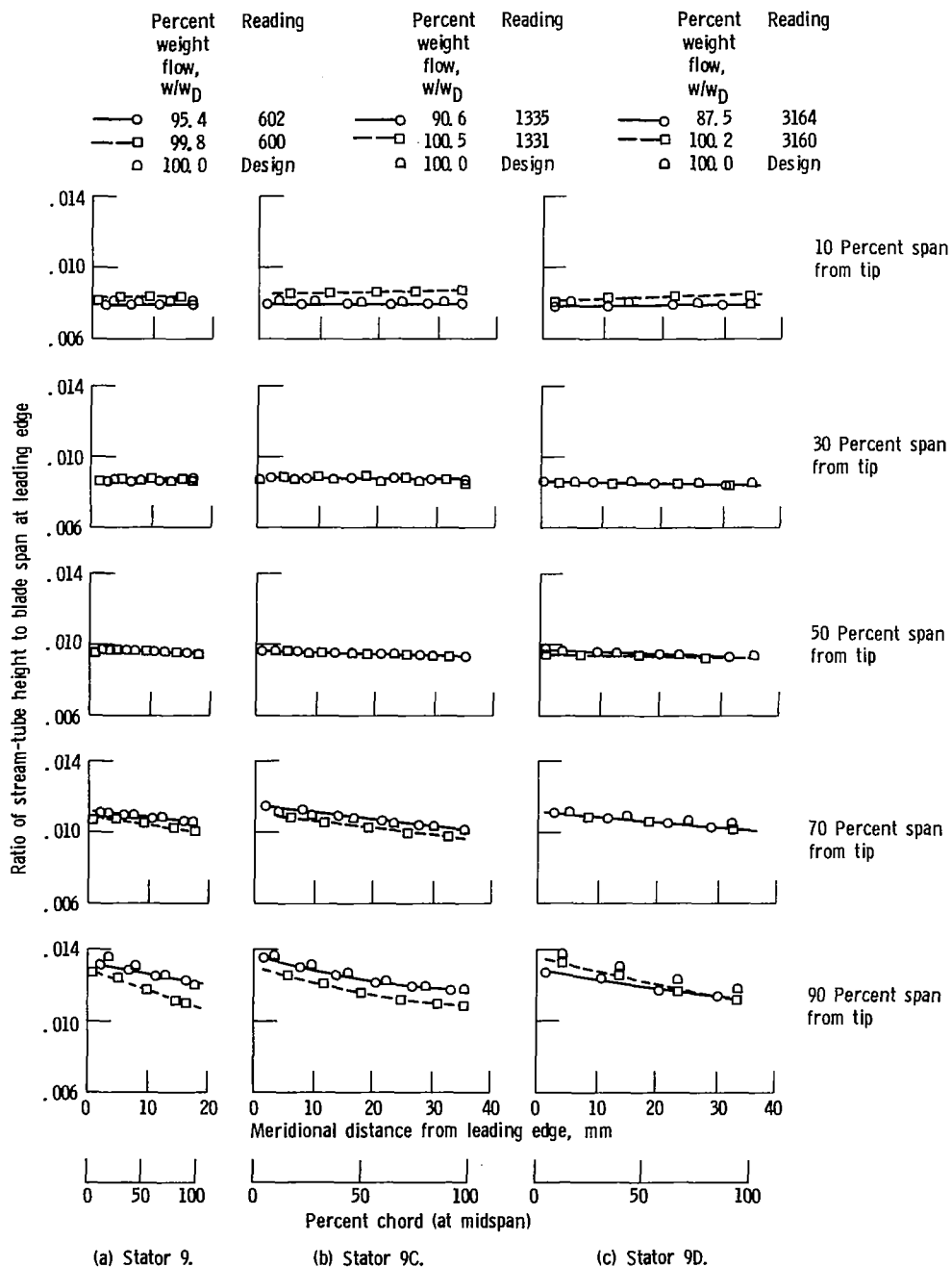


Figure 4 - Meridional distributions of stream-tube heights for S9, S9C, S9D at three weight flows and at design speed.

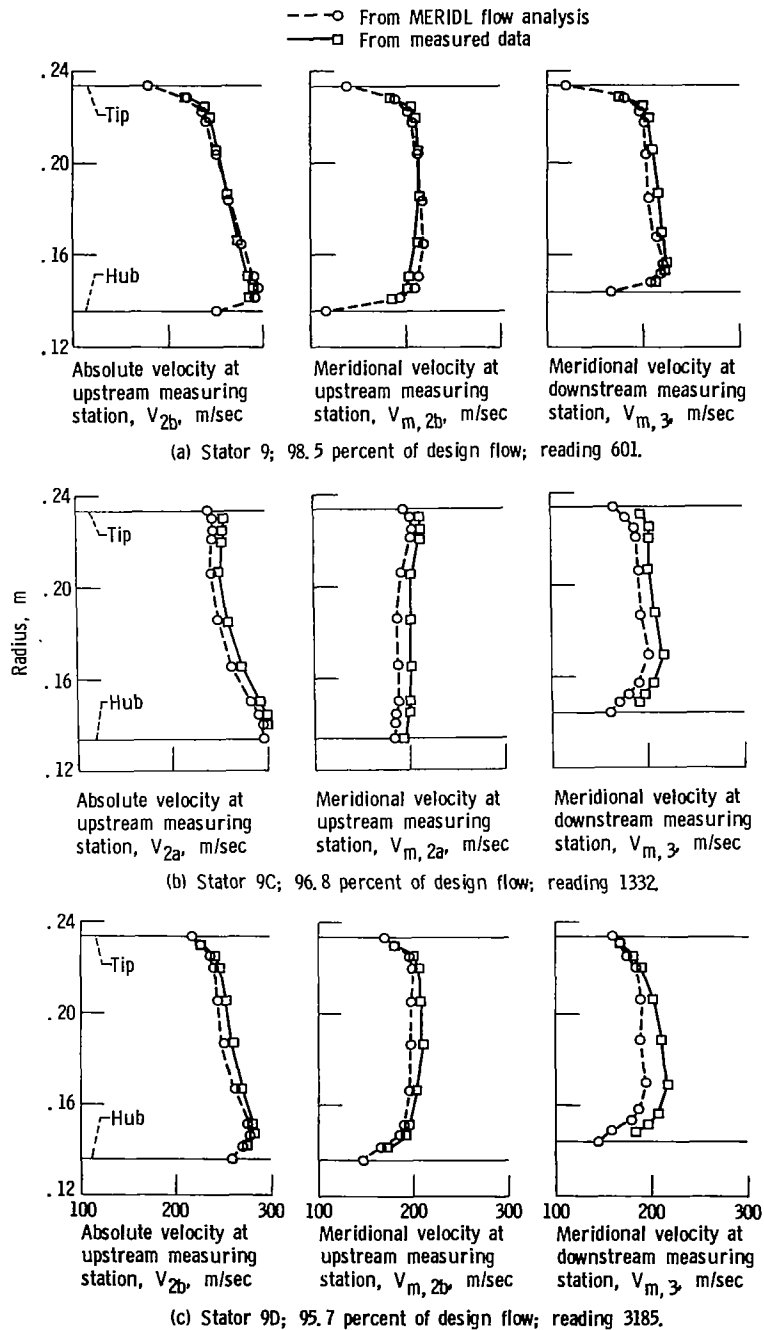


Figure 5. - Comparison of MERIDL analysis with measured data at design speed and near-peak stage efficiency.

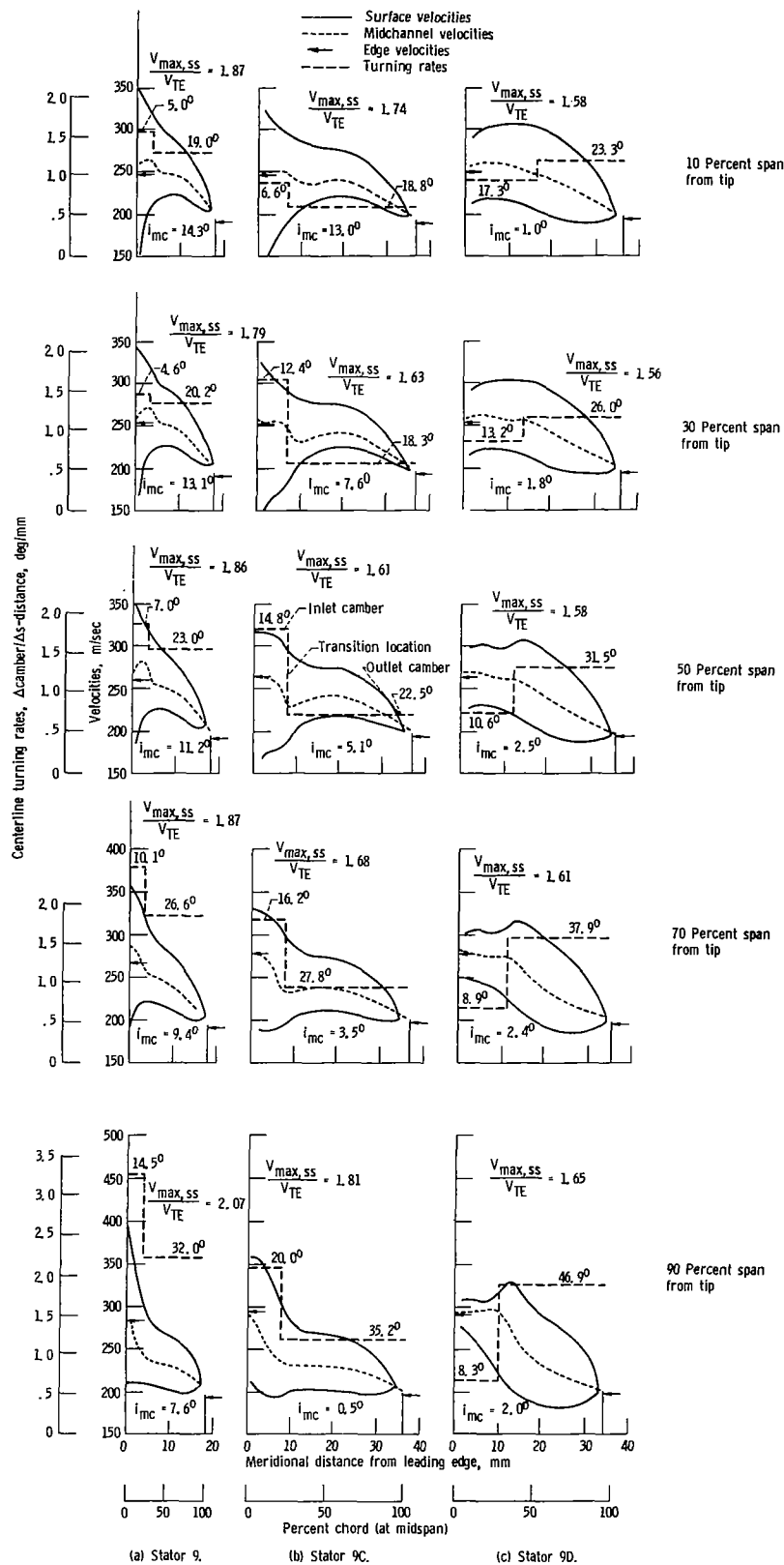


Figure 6. - Chordwise distribution of surface velocities for S9, S9C, and S9D at their design points.

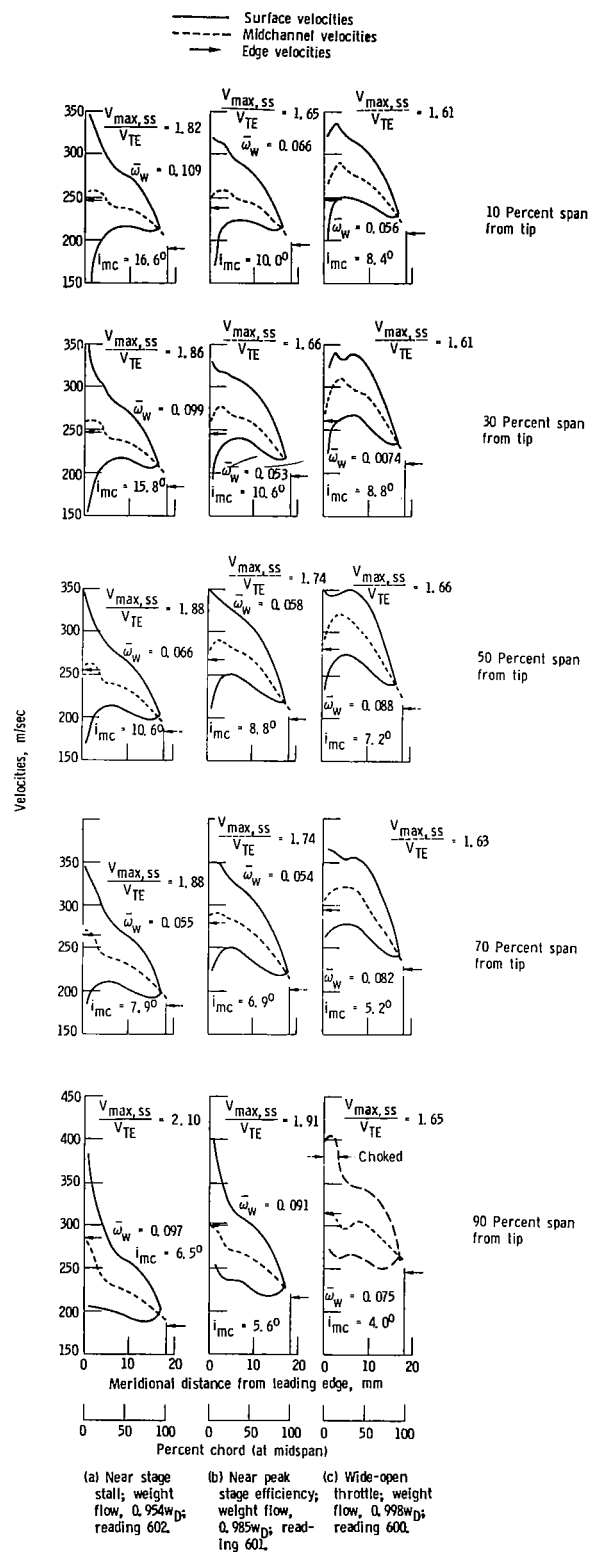


Figure 7. - Chordwise distributions of surface velocities for S9 at three weight flows and at design speed.

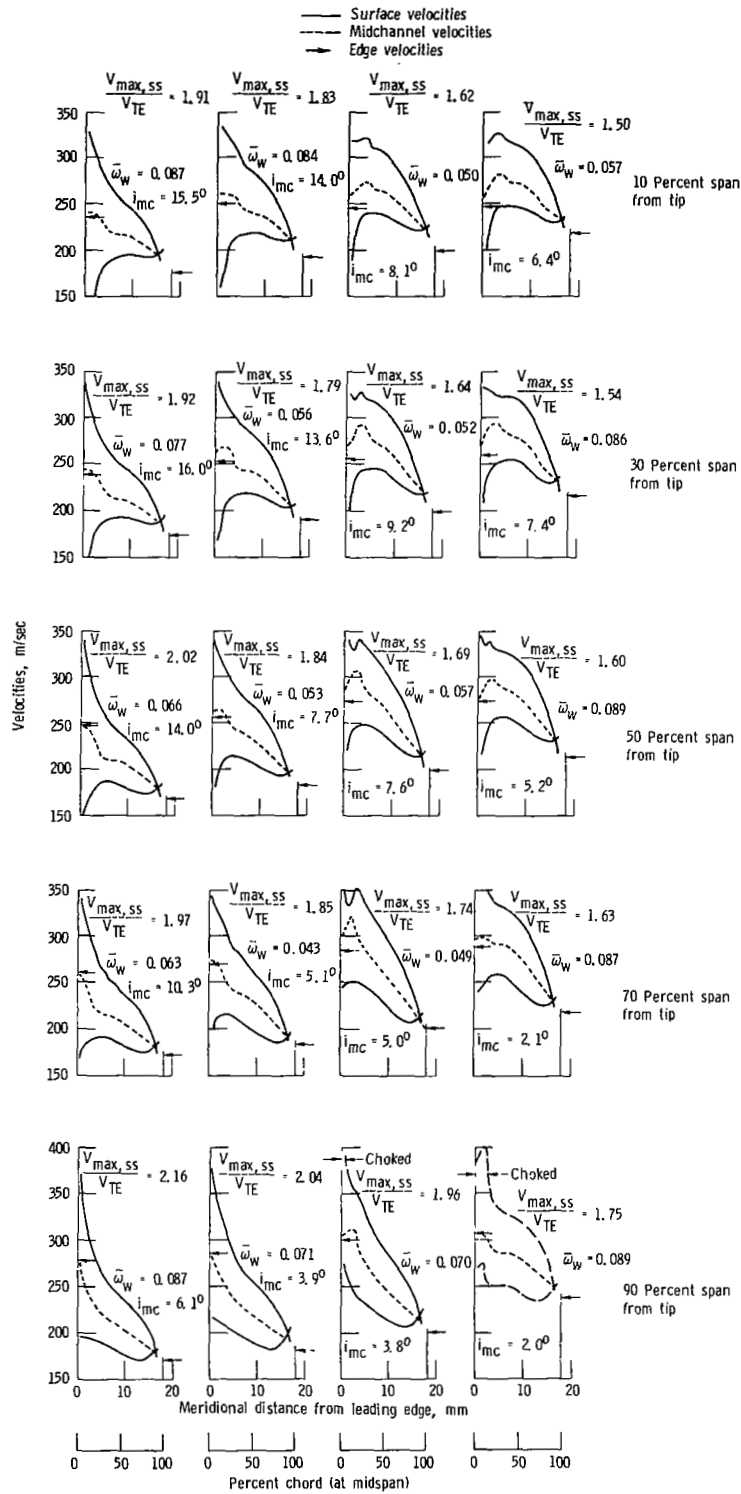


Figure 8. - Chordwise distributions of surface velocities for S9R at four weight flows and at design speed.

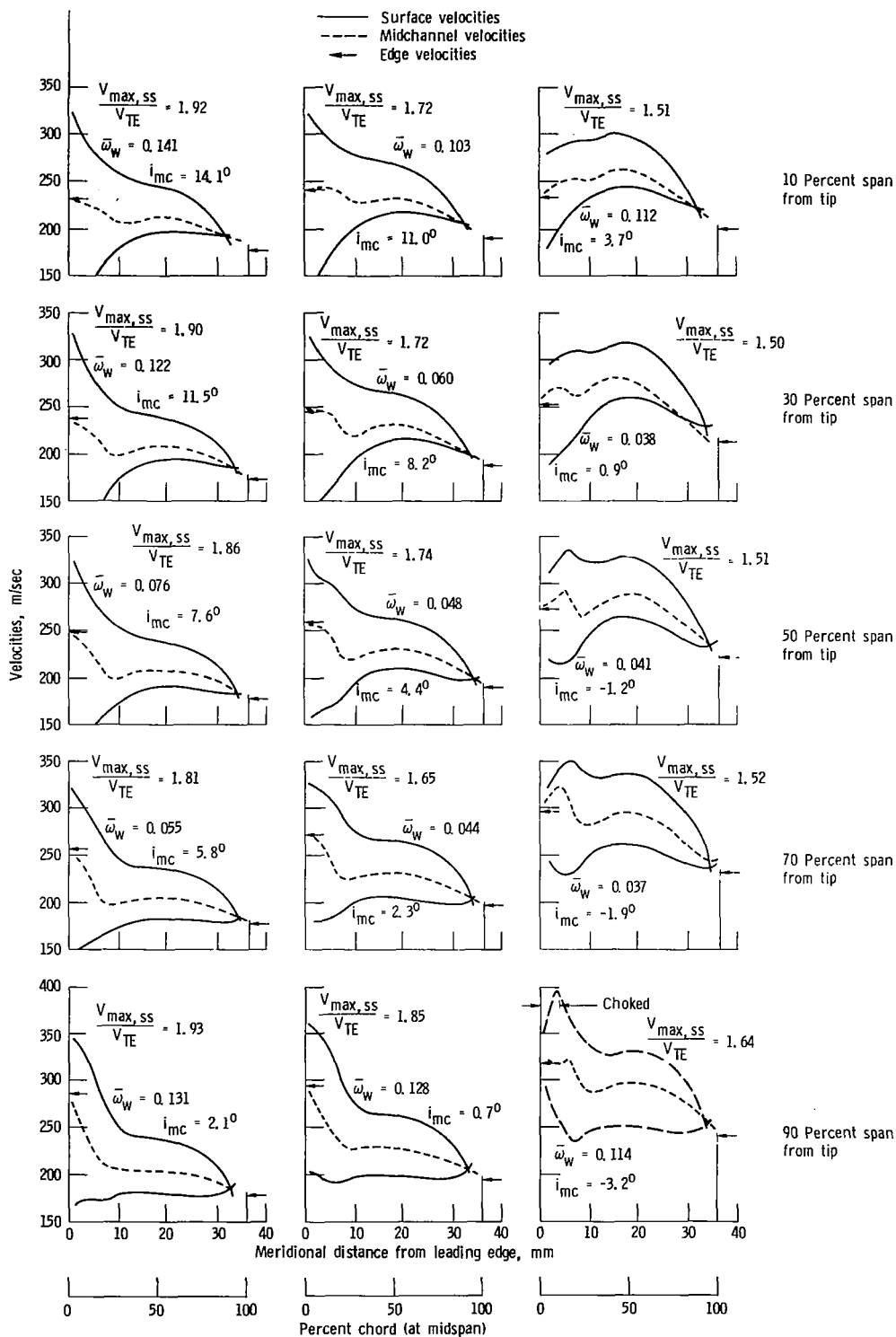


Figure 9. - Chordwise distributions of surface velocities for S9C at four weight flows and at design speed.

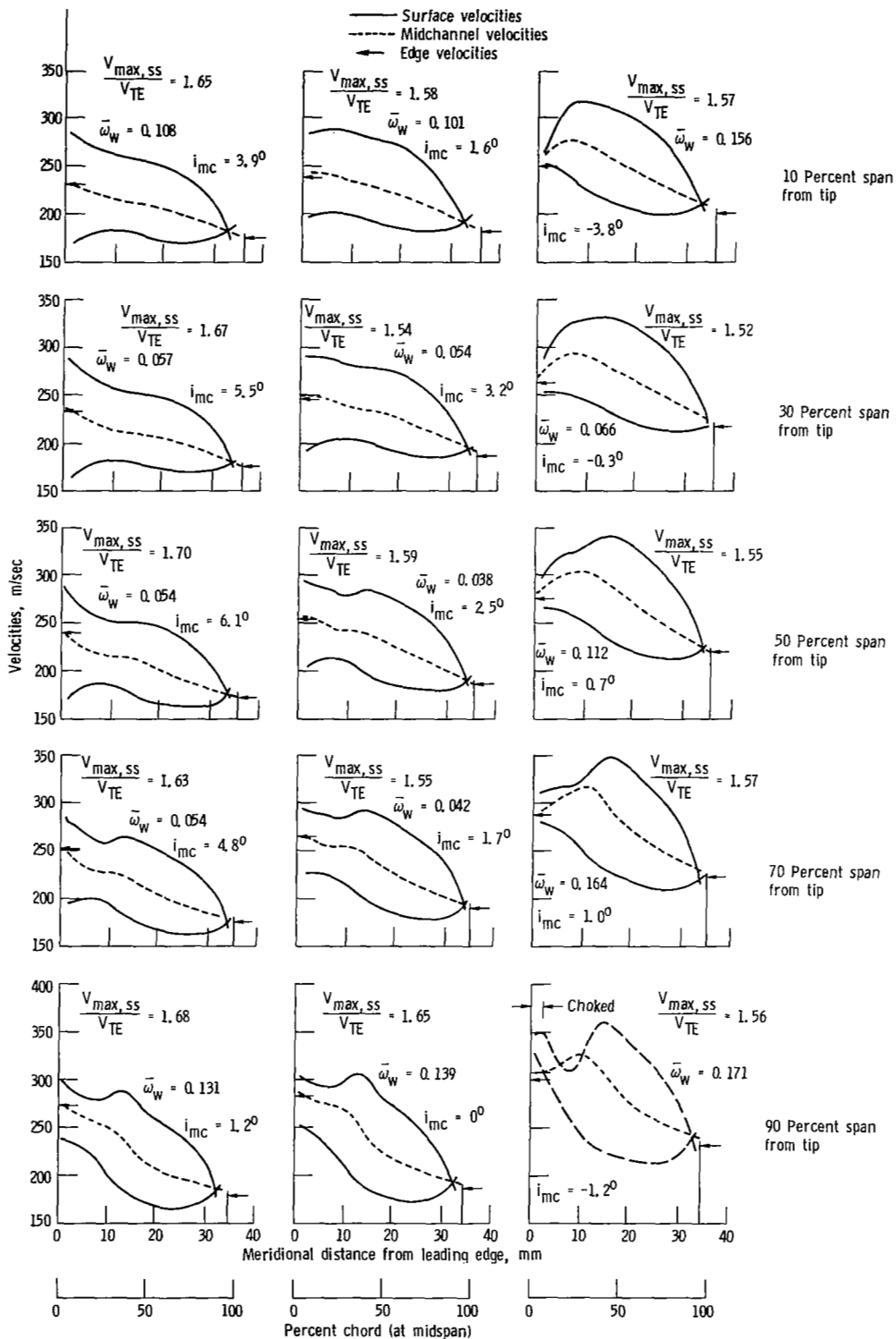


Figure 10. - Chordwise distributions of surface velocities for S9D at three weight flows and at design speed.

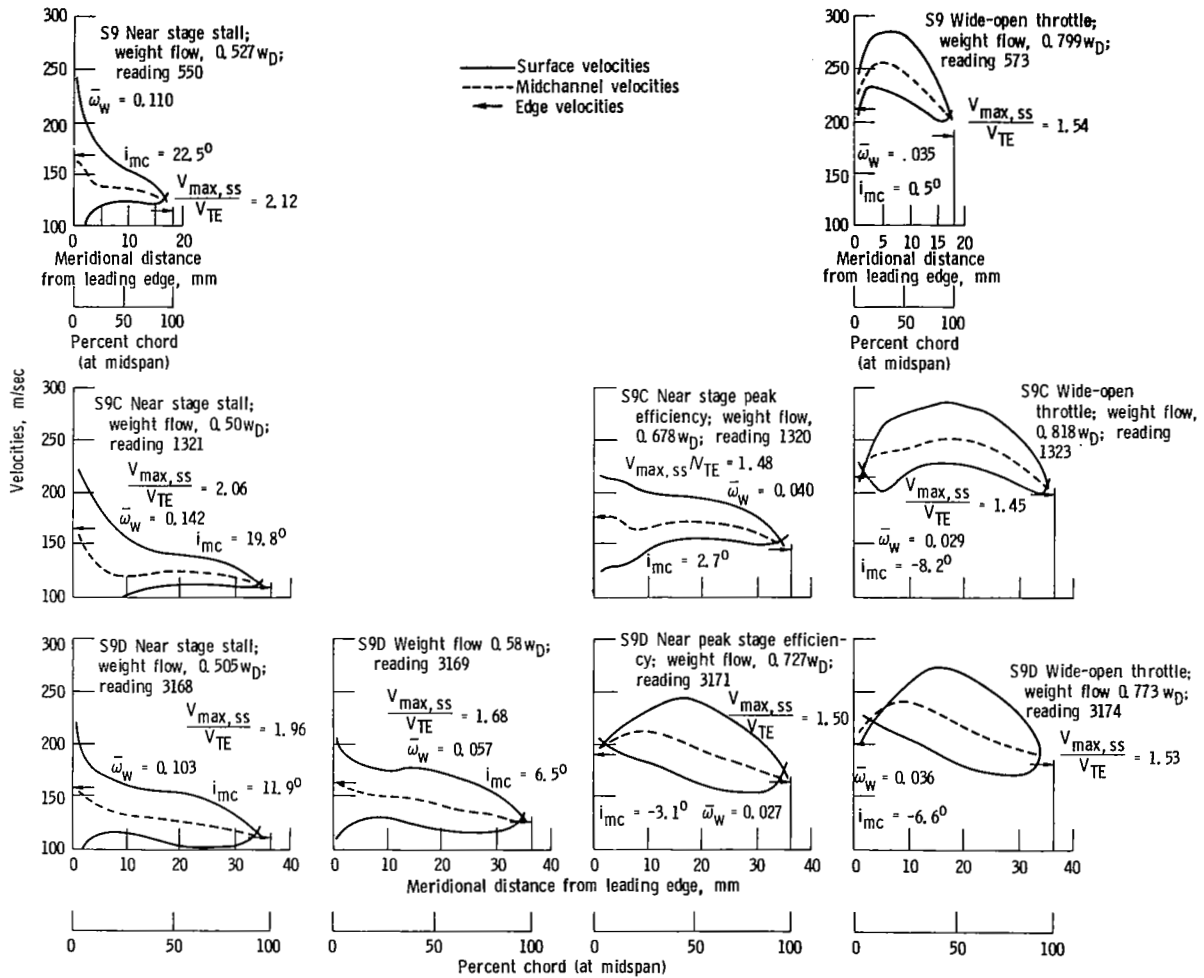


Figure 11. - Chordwise distributions of surface velocities at 50-percent span for S9, S9C, and S9D at several weight flows and at 70 percent of design speed.

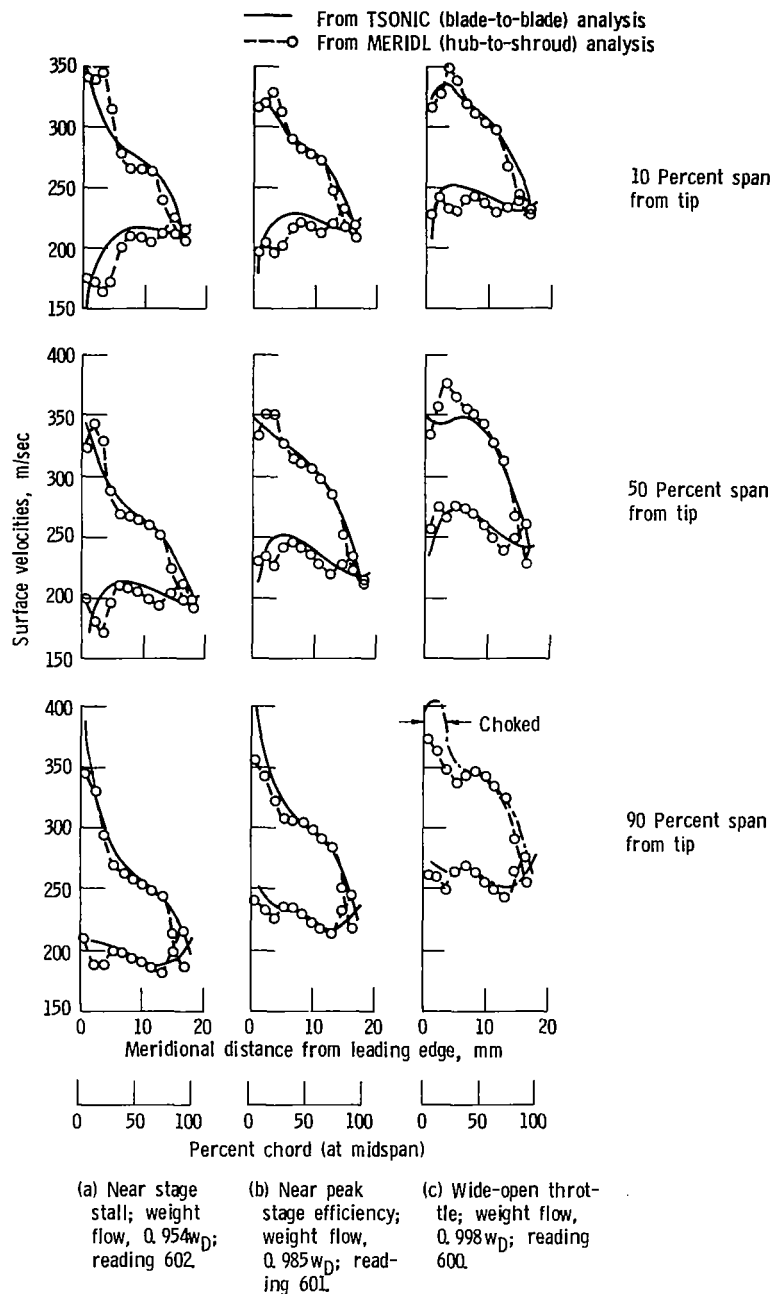


Figure 12. - Comparison of surface velocities from TSONIC with those from MERIDL for S9 at three weight flows and at design speed.

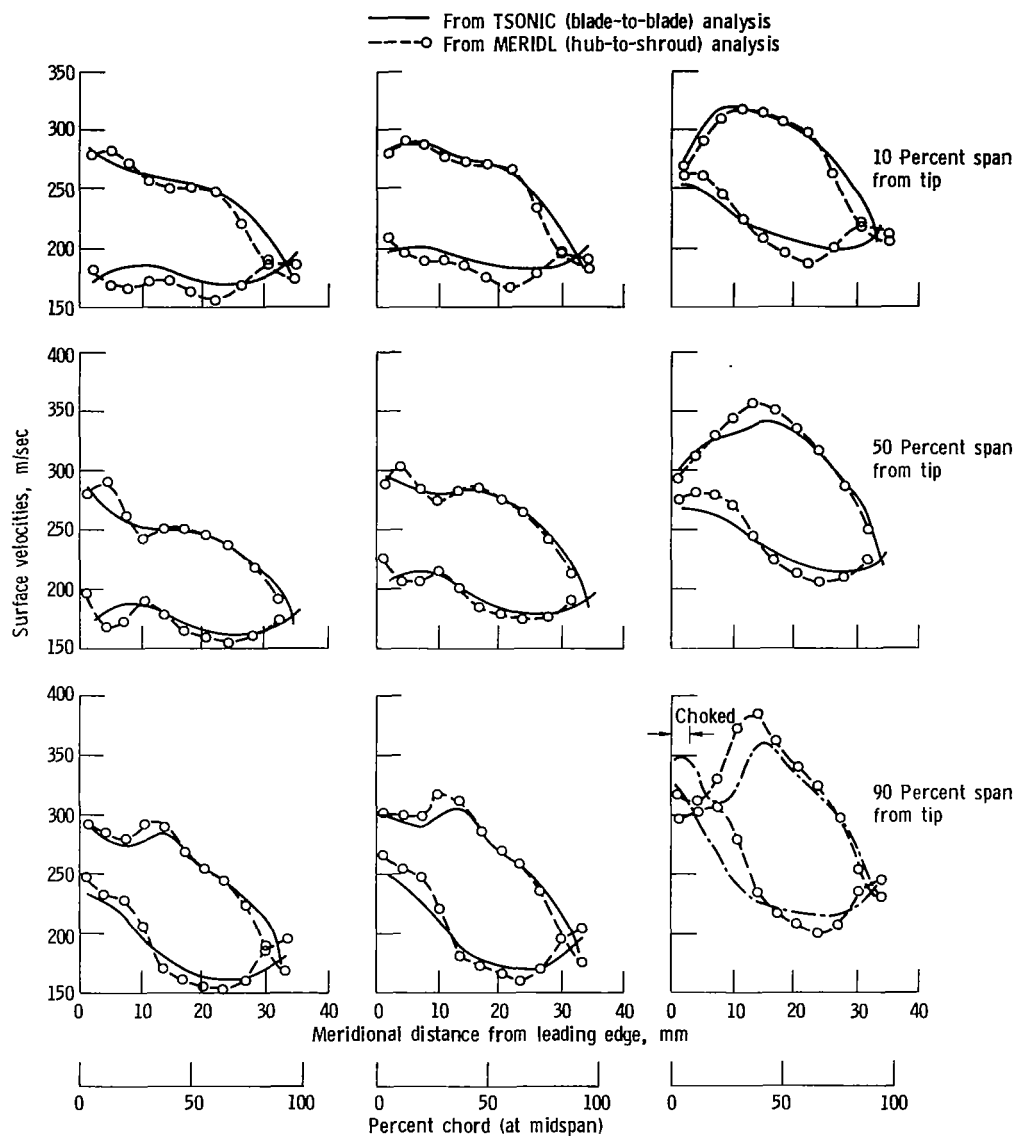


Figure 13. - Comparison of surface velocities from TSONIC with those from MERIDL for S9D at three weight flows and at design speed.

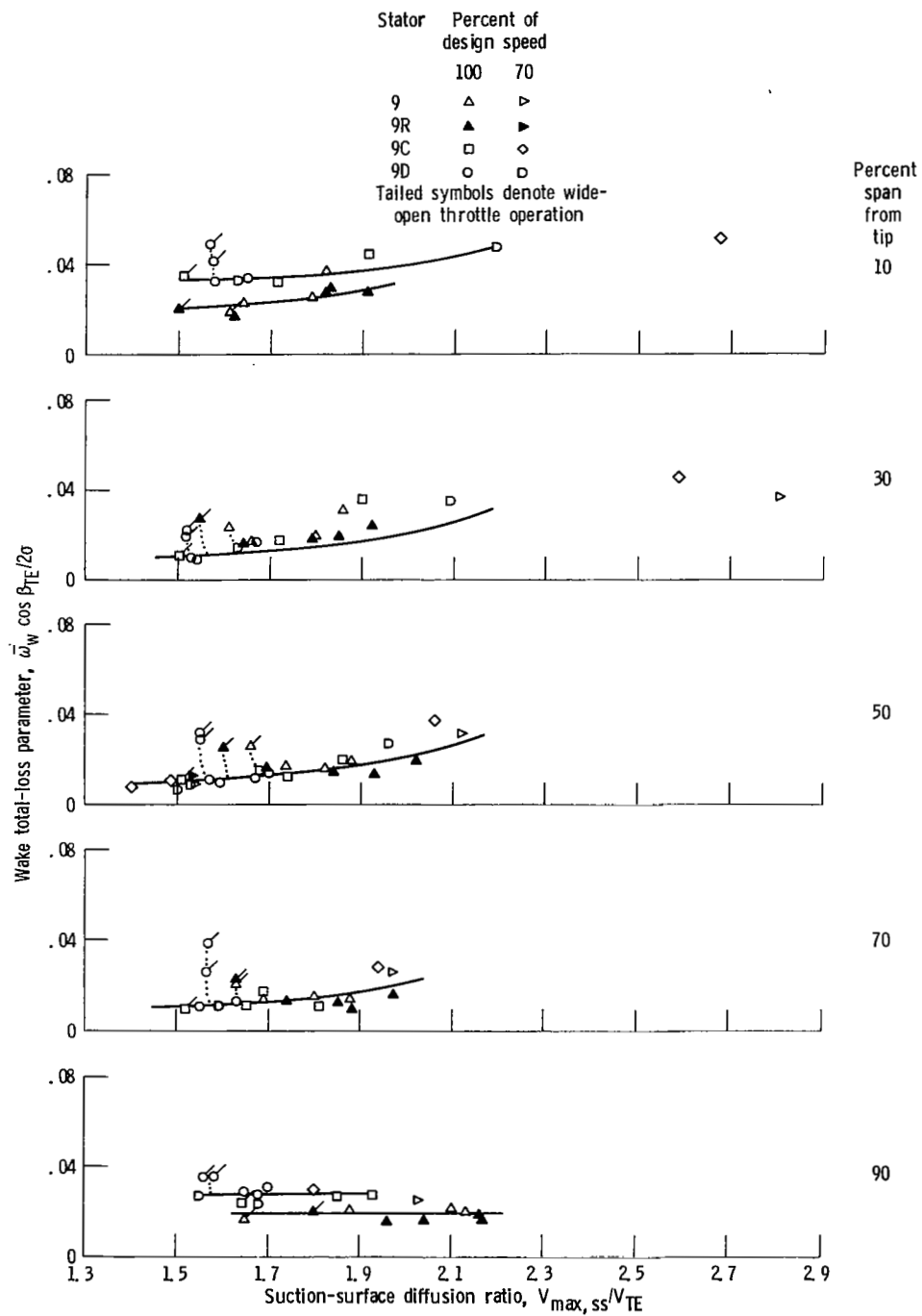


Figure 14 - Stator-loss parameter as function of suction-surface diffusion ratio calculated by internal-flow analysis.

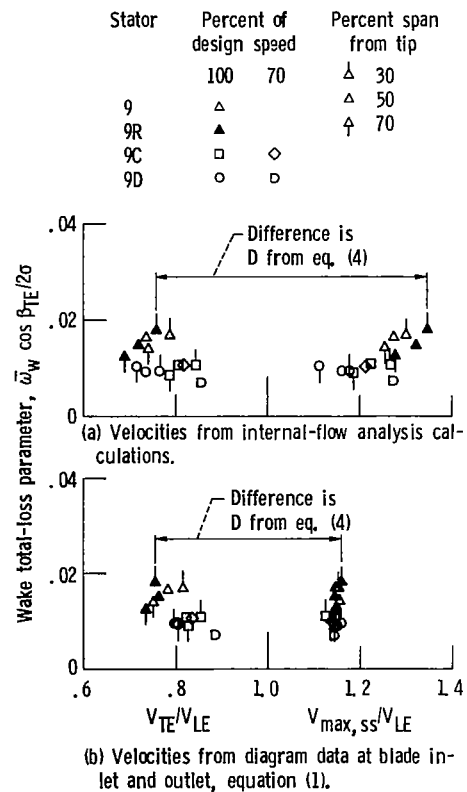


Figure 15. - Stator-loss parameter at minimum-loss operation as function of velocity ratios. Velocities evaluated with and without internal-flow analysis calculations.

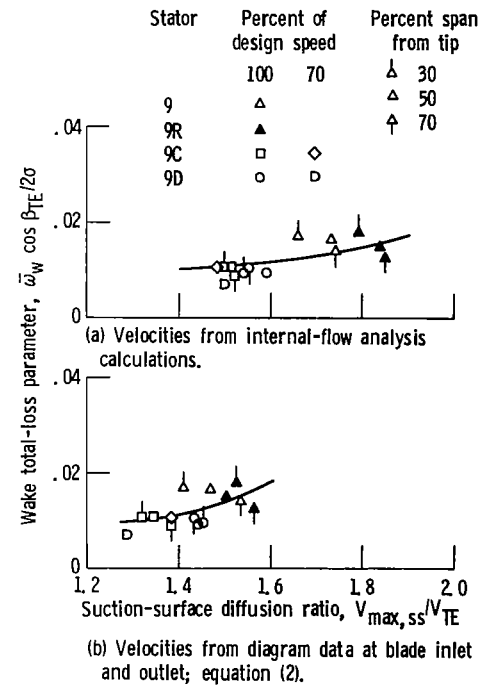


Figure 16. - Stator-loss parameter at minimum-loss operation as function of suction-surface diffusion ratio evaluated with and without internal-flow analysis calculations.

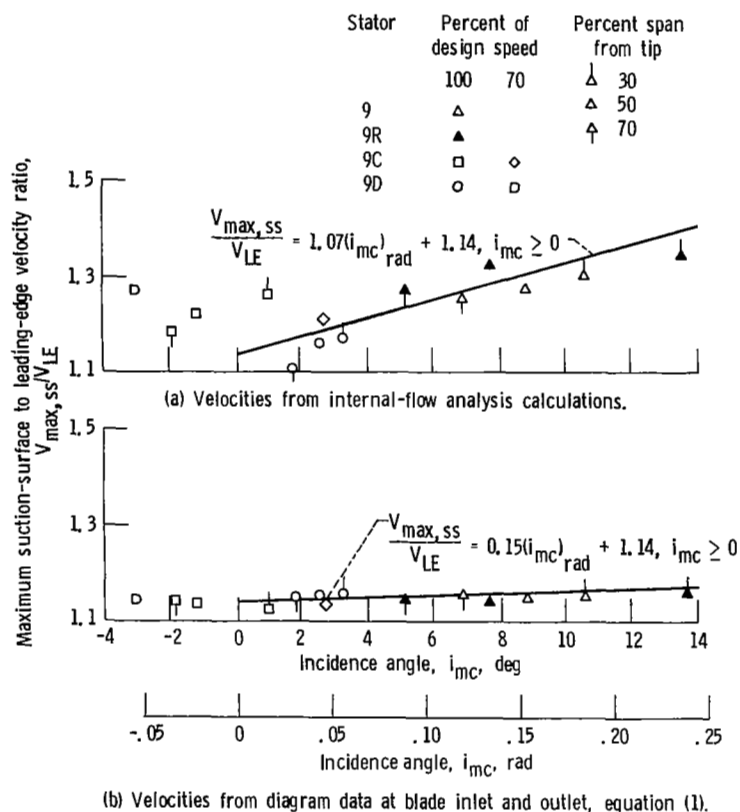


Figure 17. - Effect of incidence angle at minimum-loss operation on maximum suction-surface to leading-edge velocity ratio evaluated with and without internal-flow analysis calculations.

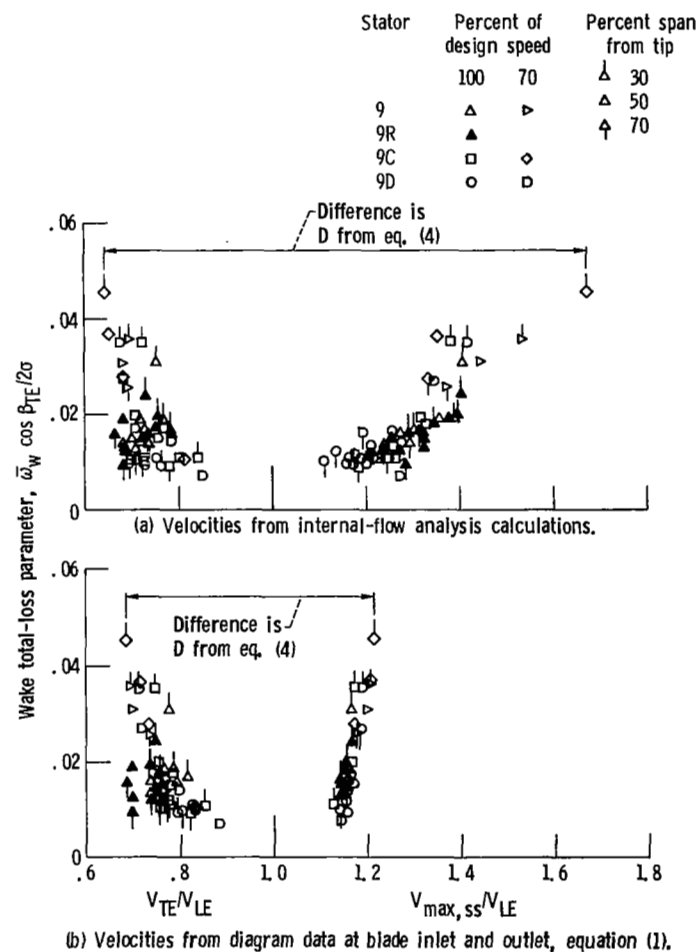


Figure 18. - Stator-loss parameter at minimum-loss to near-stall operation as function of velocity ratios. Velocities evaluated with and without internal-flow analysis calculations.

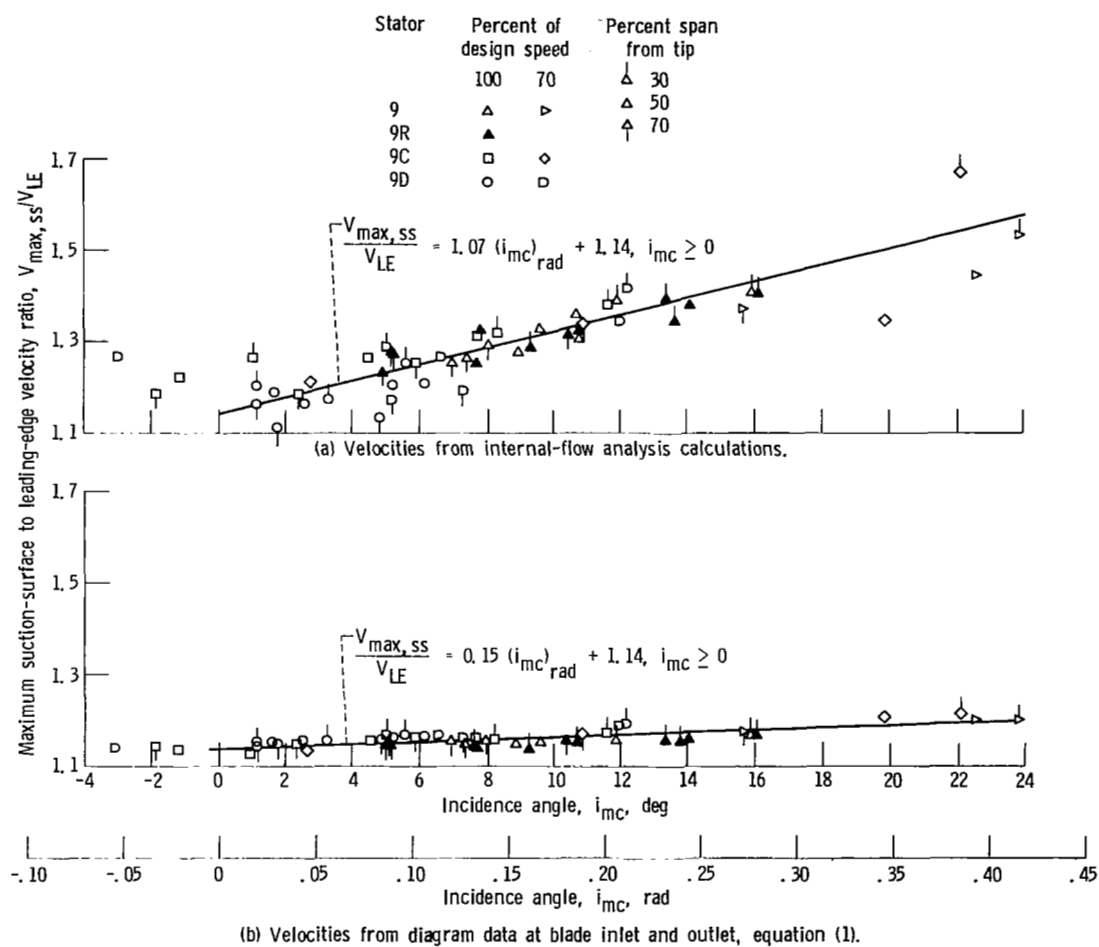


Figure 19. - Effect of incidence angle at minimum loss to near stall operation on maximum suction-surface to leading-edge velocity ratio evaluated with and without internal-flow analysis calculations.

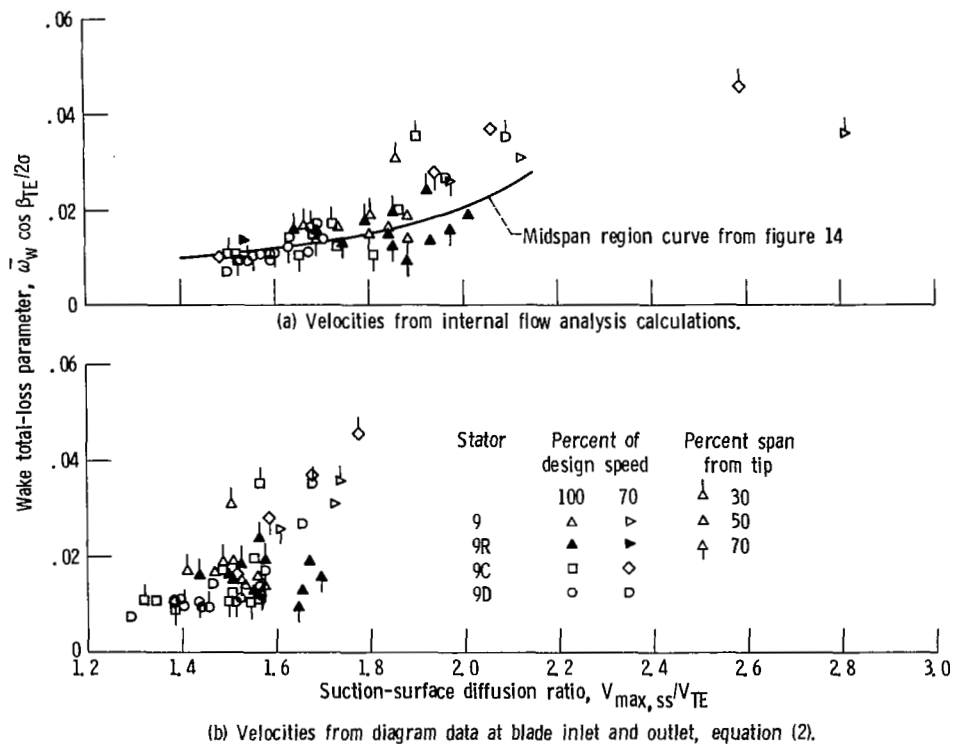


Figure 20. - Stator-loss parameter at minimum-loss to near-stall operation as function of suction-surface diffusion ratio evaluated with and without internal-flow analysis calculations.

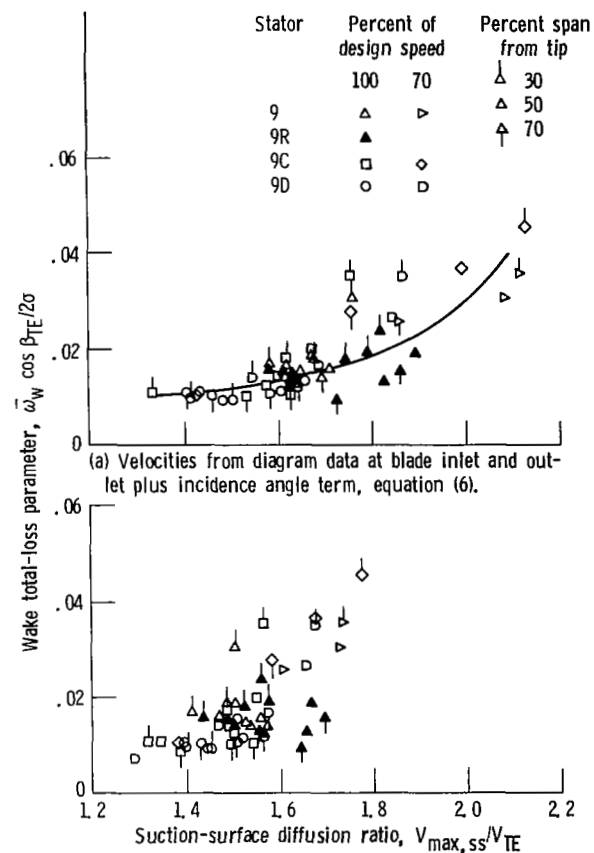


Figure 21. - Stator-loss parameter at minimum-loss to near-stall operation as function of suction-surface diffusion ratio evaluated with and without an additive incidence angle term.

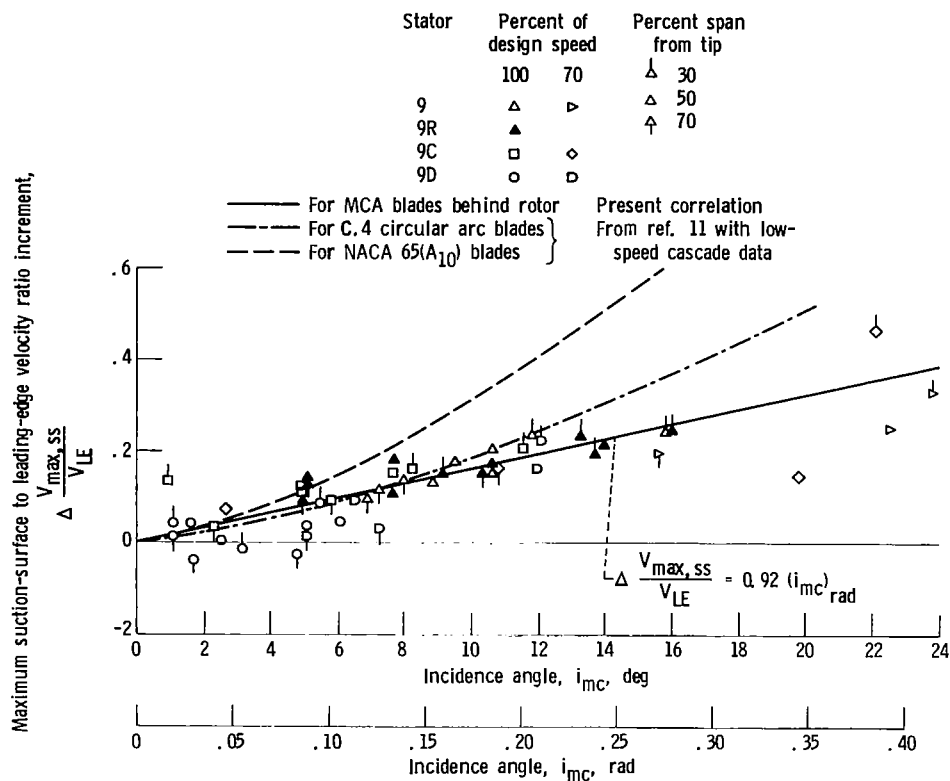


Figure 22 - Comparison of correlations for effect of off-design incidence angle on maximum-suction-surface to leading-edge velocity ratio increment above minimum loss levels.

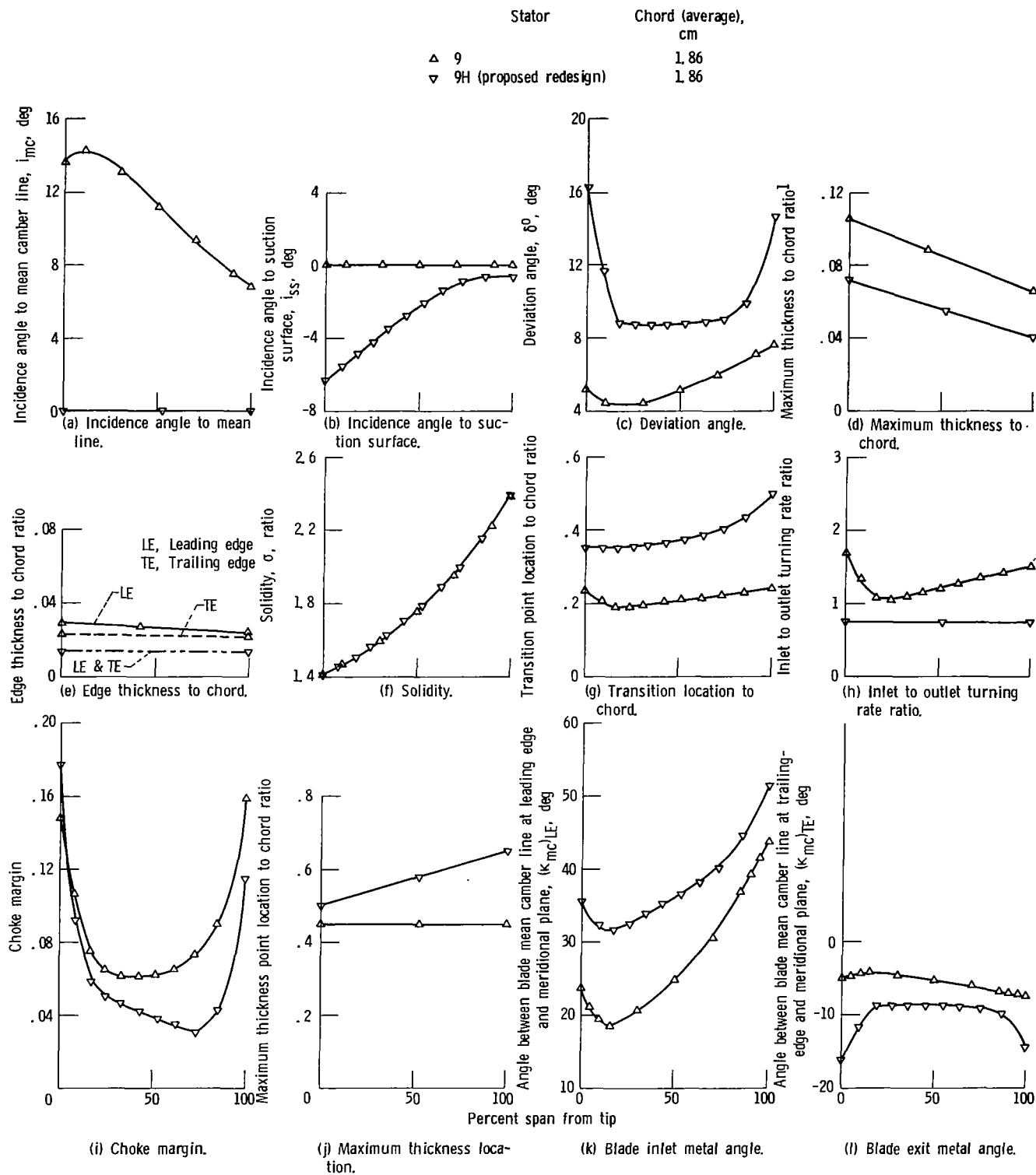


Figure 23. - Comparison of design parameters for S9H and S9. (Edge thickness to chord ratio and choke margin include 0.0086-cm wrap on S9 (see ref. 1).)

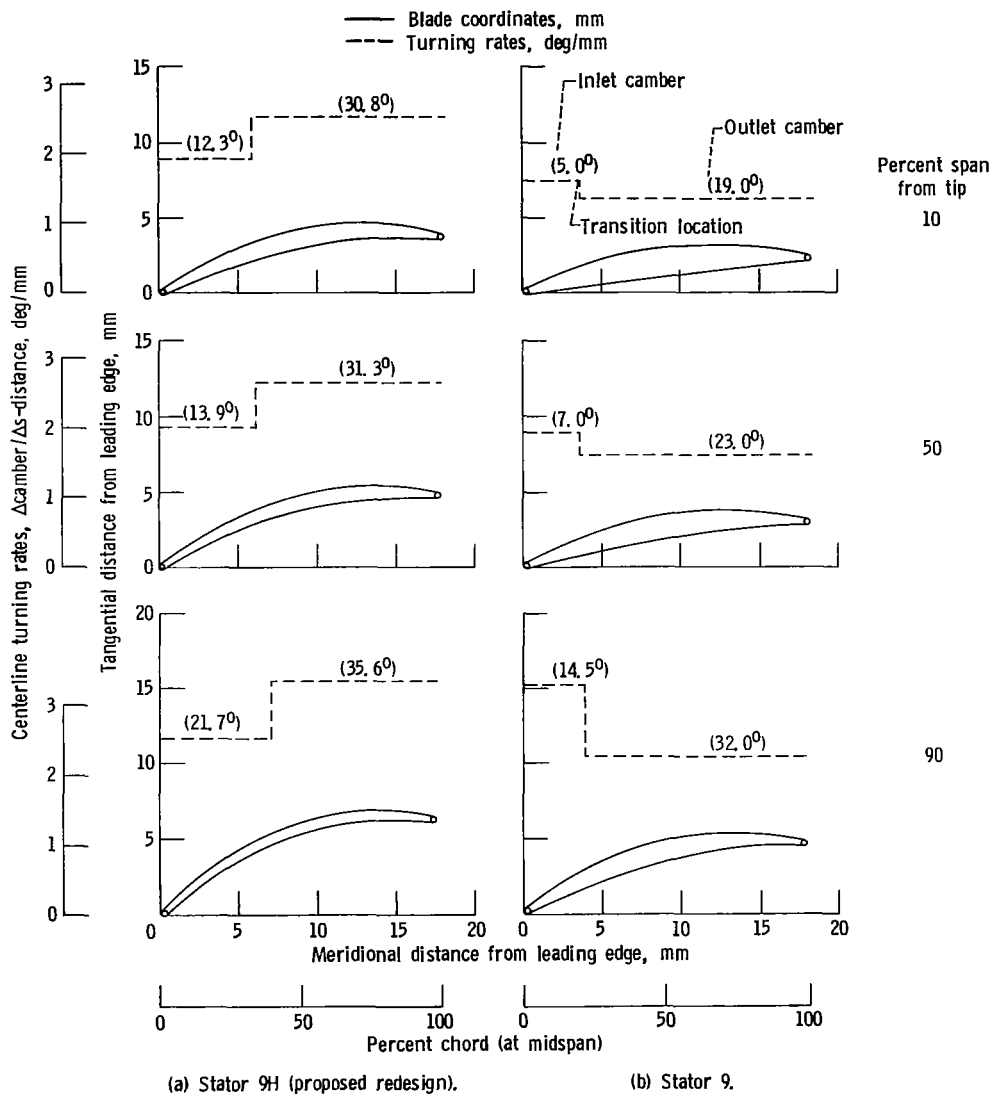
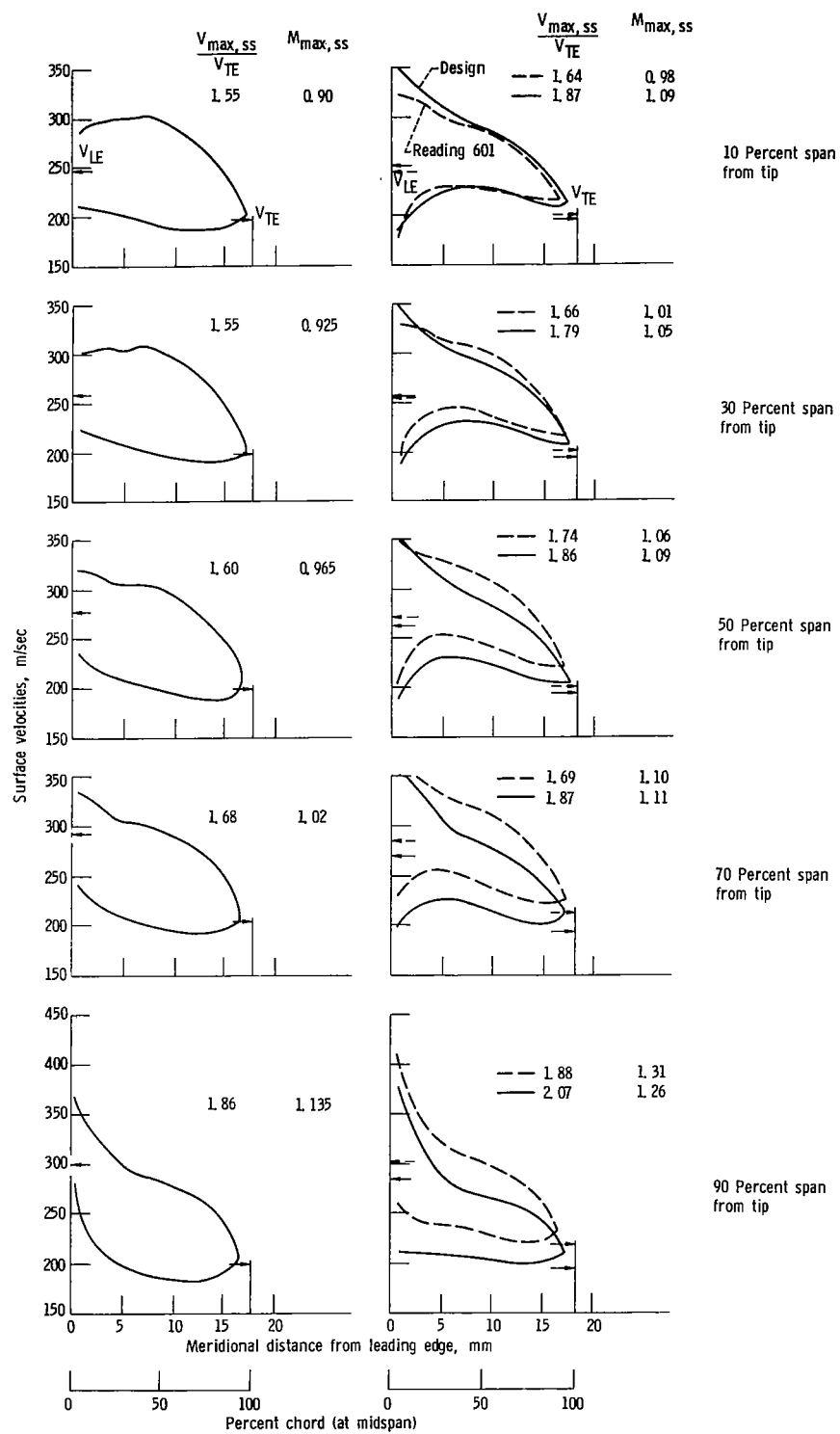


Figure 24. - Comparison of blade shapes for S9H and S9.



(a) Stator 9H (proposed redesign based on reading 704, ref. 1).

(b) Stator 9 (tested).

Figure 25. - Meridional distribution of surface velocities at five spanwise locations for S9H (proposed redesign) compared with S9 design and its best performance test point.

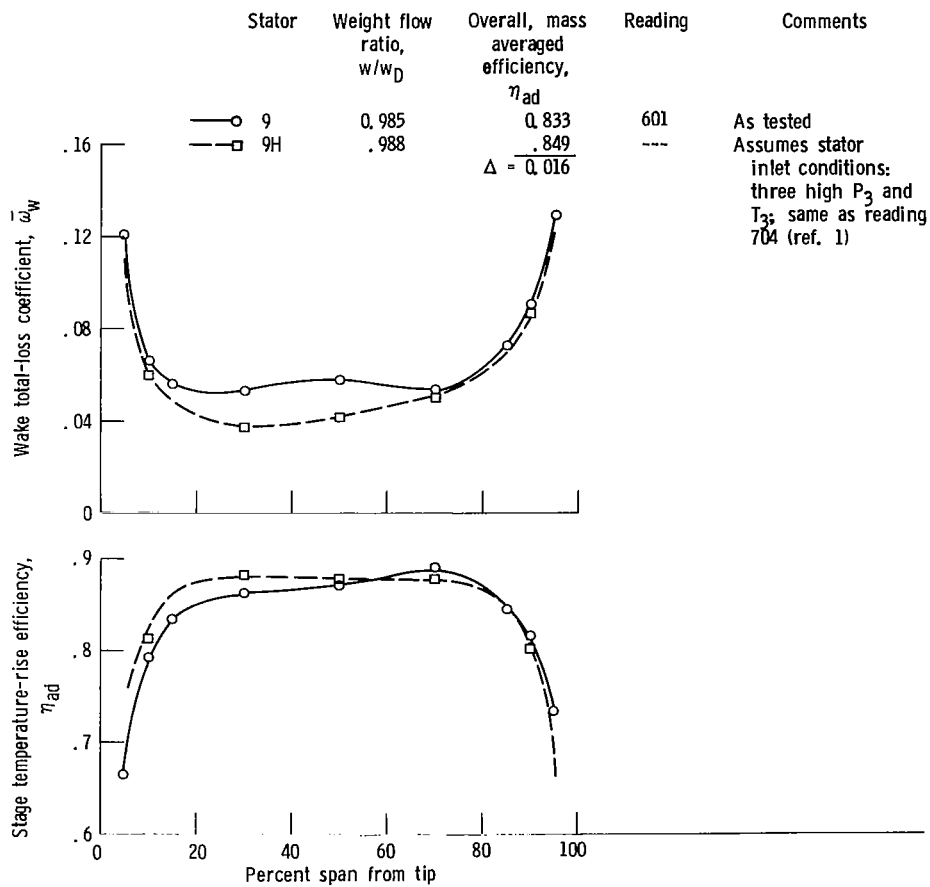


Figure 26. - Effect of S9 redesign (S9H) on performance (estimated).

1. Report No. NASA TP-1614		2. Government Accession No.		3. Recipient's Catalog No.	
4. Title and Subtitle AERODYNAMIC PERFORMANCES OF THREE FAN STATOR DESIGNS OPERATING WITH ROTOR HAVING TIP SPEED OF 337 METERS PER SECOND AND PRESSURE RATIO OF 1.54 II - RELATION OF ANALYTICAL CODE CALCULATIONS TO EXPERIMENTAL PERFORMANCE				5. Report Date April 1980	
				6. Performing Organization Code	
7. Author(s) Thomas F. Gelder, James F. Schmidt, and Genevieve M. Esgar				8. Performing Organization Report No. E-137	
9. Performing Organization Name and Address National Aeronautics and Space Administration Lewis Research Center Cleveland, Ohio 44135				10. Work Unit No. 505-04	
				11. Contract or Grant No.	
12. Sponsoring Agency Name and Address National Aeronautics and Space Administration Washington, D.C. 20546				13. Type of Report and Period Covered Technical Paper	
				14. Sponsoring Agency Code	
15. Supplementary Notes					
16. Abstract <p>A hub-to-shroud and a blade-to-blade internal-flow analysis code, both inviscid and basically subsonic, were used to calculate the flow parameters within four stator-blade rows. The code-produced ratios of maximum-suction-surface velocity to trailing-edge velocity correlated well in the midspan region, with the measured total-loss parameters over the minimum-loss to near-stall operating range for all stators and speeds studied. The potential benefits of a blade designed with the aid of these flow analysis codes are illustrated by a proposed redesign of one of the four stators studied. An overall efficiency improvement of 1.6 points above the peak measured for that stator is predicted for the redesign.</p>					
17. Key Words (Suggested by Author(s)) Turbomachinery			18. Distribution Statement Unclassified - unlimited STAR Category 07		
19. Security Classif. (of this report) Unclassified		20. Security Classif. (of this page) Unclassified		21. No. of Pages 52	
				22. Price* A04	